MODELING AND OPTIMAL CONTROL OF CURVATURES IN IPMC'S

A Thesis
Submitted to the Graduate Faculty
of the
North Dakota State University
of Agriculture and Applied Science

By

Smriti Tripathi

In Partial Fulfillment of the Requirements
for the Degree of
MASTER OF SCIENCE

Major Department:
Mechanical Engineering

October 2014

Fargo, North Dakota

North Dakota State University
Graduate School

Title

Modeling and Optimal Control of Curvatures in IPMC's

By

Smriti Tripathi

The Supervisory Committee certifies that this ***disquisition*** complies with North Dakota State University's regulations and meets the accepted standards for the degree of

MASTER OF SCIENCE

SUPERVISORY COMMITTEE:

Dr. Majura Selekwa
Chair

Dr. Yildirim Bora Suzen

Dr. Annie Tangpong

Dr. Om Yadav

Approved:

11/24/2014 — Date

Dr. Alan Kallmeyer — Department Chair

ABSTRACT

There has been a growing number of research activities in the area of using smart materials in day to day lives because of their ability to serve both as sensors and actuators. Ionic Polymer Metal Composites (IPMCs) are one of such materials which have been extensively studied in the past few decades to not only understand its working principles but to also model and control their curvature. The problem of building an electromechanical model in order to explain the functioning of IPMCs under favorable and unfavorable conditions is still unsolved. This work proposes a control oriented electromechanical model for induced bending curvature in the IPMC material based on the empirical data received on Nafion based IPMC specimen. This model is further utilized to formulate a control oriented dynamic model from which an Optimal Control System was suggested for the IPMC actuator and supported by experimental results on the tip displacement.

ACKNOWLEDGMENTS

I would like to sincerely thank my academic advisor Dr. Majura Selekwa for guiding me and for the continued support throughout the research. I have been able to learn a lot from him while working as his teaching assistant and research assistant. His knowledge and understanding of various distinct technical fields has always amazed and inspired me to work harder.

I would also like to thank Dr. Om Prakash, Dr. Bora Suzen and Dr. Annie Tangpong for their valuable advice and for serving as committee members.

TABLE OF CONTENTS

LIST OF TABLES

LIST OF FIGURES

Figure Page

1. INTRODUCTION

1.1. Research Objectives

The primary objective of this research is to develop a model that can be utilized in accurately controlling the IPMC bending. The major contributions of this research are as follows:

1. The step response of the IPMCs held in a cantilever position were analyzed.
2. The experimental data received on the unit step response time history of the electric current flowing across the specimen was used to develop an electrical model.
3. Based on the experimental data received on the tip deflection to a unit step voltage, a mechanical model was developed.
4. The electrical and mechanical models were combined to validate the electromechanical coupling experienced by the IPMC actuator.
5. The electromechanical model was then used to formulate a control oriented dynamic model of a Nafion based IPMC specimen from which an Optimal Control System was suggested for the IPMC actuator and supported by experimental results on the tip displacement.

1.2. Background

Actuators are devices that make things move; they are necessary as sources of driving forces and displacements for a range of applications that require mechanical actions as found in various phenomena that occur either naturally or artificially. Actuators are found in almost everything that involves motion in our surroundings. There are biological actuators that stimulate movement in our body parts, and engineering actuators as found in many engineering systems such as aerospace, automotive, industrial and medical equipment. Typical examples of naturally occurring actuators are muscles in human beings, animals and plants whereas examples of man-made actuators include electrical and fluid power motors, and electrical solenoids. An actuator is

a device that assimilates energy from one or more sources and converts it into mechanical motion in a controlled way. This motion can cause many effects such as clamping, blocking or ejecting. Most engineering actuators usually take energy in the form of electricity, fluid motion or chemical reactions and produce motion either in linear, rotary or oscillatory form.

The performance of an actuator is primarily characterized by its response speed, force capacity, operating range and energy efficiency; however, other parameters such as mass, tolerance to different operating conditions, controllability and the sensor's specific volume also play crucial roles in characterizing the quality of the actuator. As the demand for miniatun rized devices increases to grow, it has led to an increased interest in smaller, more energy efficient, and highly accurate actuators. As such there have been a growing number of research activities in unconventional actuator materials. In this effort, materials that simultaneously offer both sensing and actuation characteristics, also known as smart materials, have attracted more interest because of their ability to serve as both actuators and feedback sensors, which offer possibilities for reduction in both size and energy consumption. Today, popular smart materials include piezoelectric materials, shape memory materials, magnetostrictive materials and electroactive polymers (EAPs).

While piezo materials, shape memory materials and magnetostrictive materials have been extensively studied and developed, Electroactive polymer materials are still the least developed and understood. First patented in 1993 [1], EAPs are a class of polymeric smart materials that display significant change in shape and size when subjected to applied electric fields, and also generate electric fields under application of mechanical stress. EAPs are generally classified into two groups based on their actuation mechanisms: electronic and ionic. Electronic EAPs include electrostatic, electrostrictive, ferroelectric and piezoelectric polymers [45]. Their actuation

mechanisms are caused by electrostatic forces between two electrodes across the material. These forces squeeze the polymer, leading to a mechanical deformation, these polymers require high activation voltages, and their displacements are easily controllable since they can hold and retain the induced displacement under the applied DC voltage for a long time [10]. On the other hand, Ionic electroactive polymers have an actuation mechanism caused by the displacement of foreign solvent ions within the polymer membrane itself. Generally, these polymers are only active when wet so for the foreign ions to be present; they require low actuation voltage (in the range of 1V to not more than 5V) and offer high displacement/voltage ratios compared to electronic EAP. Because of the inherent wetness condition, displacements of ionic electroactive polymer actuators are generally difficult to control and stabilize except in the case for carbon nanotubes and conductive polymers [45]. Popular ionic EAPs include ionic gels, ionic polymer metal composites, conducting polymers and carbon nanotubes. Because of their good response to low actuation voltage levels, ionic polymers have very promising applications in many handheld devices; as such there has been a growing interest in understanding their mechanics and developing better ways of controlling their displacements.

An ionic polymer metal composite (IPMC) is a type of ionic EAP which comprises of a perfluorinated membrane sandwiched between two metal electrodes with high conductive surface layer attached as shown Fig.1. [8]. Each of its surface electrodes is made of two coatings; the first coating is of dispersed small platinum particles embedded inside the surface of the membrane and the second is the gold coating at the surface in order to enhance its conductivity.

As smart materials, IPMCs display strong bidirectional electromechanical coupling i.e., they generate voltage across their cross sections when subjected to mechanical deformation and also they undergo mechanical deformation when subjected to electrical fields [7]. IPMCs have

been of more interest to researchers because of their ability to provide large displacements at low activation voltages; additionally, they offer great force to weight ratio and can be easily cut and used as micro actuators. In general, IPMCs have shown immense potential to be used as electro-dynamic sensors, artificial muscles and soft robotic actuators [9].

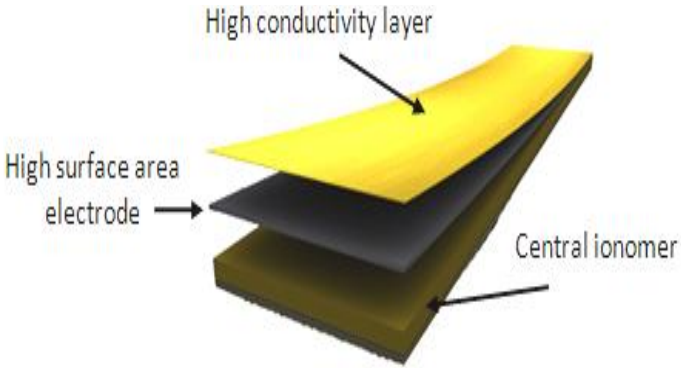

Fig. 1. Structure of ionic polymer metal composites [8]

1.3. A Brief History of IPMCs

Work on EAPs started in early 1880s, and the first experiment that involved an EAP was performed by Roentgen in 1880 [62] while investigating the effects of electric current on the mechanical properties of a rubber band. A rubber-band was held in the cantilever position fixed at one point and attached with a mass at the free end; it was then charged and discharged to see if it could change its length because of the applied current. Despite the presence of this early work, the largest amount of work with IPMCs began in the late 1990's after the formation of the SPIE (Society of Photo-Optical Instrumentation Engineers) conference on EAPs in 1999. IPMCs gained international recognition through this conference, and came in the limelight for their potentials [68].The sensing and actuation capabilities of IPMC EAPs were discovered by two different groups in early 1990's. The sensing capabilities of IPMCs were first found in 1992 by

Sadeghipour and co-workers [51] in USA while investigating on the sensorial properties of smart materials. In that work, the researchers developed an accelerometer using Platinum plated Nafion, and used it as a vibration sensor. Experimental results of that work showed that voltage was generated when load was applied to the cell of Nafion membrane sandwiched between two metals [17]. While this group was very close to discovering the actuation capabilities of IPMC's as well, in the same year another group of researchers in Japan (Oguro and co-workers [52] [51])became the first to report it. This group, which had investigating the electrical behavior of a thin ion-conducting membrane coated with metal electrodes, found out that the membrane exhibits a large mechanical deformation when stimulated with an electric voltage.

Since then, many research groups across the world have been working on improving IPMC manufacturing procedures for better actuation capacities while also exploring their new applications [9]. In USA, researchers like Majorrad and Shahinpoor [63] have been working on improving the performance of Nafion-based IPMC actuators by optimizing the manufacturing techniques, electrode morphology, size and dimensions. Over the last decade, Ionic Polymer metal composites have increasingly attracted more research interests because of their capability to produce large strains and reasonable stress under small applied electric field.

1.4. The Basic Structure of IPMCs

An IPMC specimen is a thin (200 μm) perfluorinated ion exchange base membrane sandwiched between two noble metal electrodes, usually gold or platinum (5-10 μm thick), plated on its sides [6]. This structure is illustrated in Fig.2.

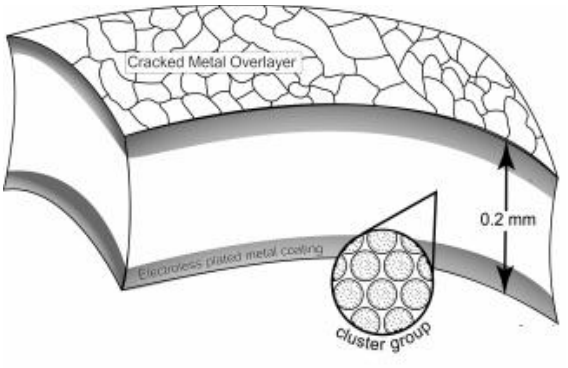

Fig. 2. IPMC dissection showing surface morphology, interface and cluster structure [6]

Popular base membranes found on most IPMCs are either the Flemion (perfluorocarboxylate made by Asahi Glass, Japan) or the Nafion (perfluorosulfonatem made by Dupont, USA) [10]. This research used a Nafion based IPMC specimen with the chemical structure shown in Fig.3. It is the most popular ion exchange membrane found in most IPMC applications. It is made of arrays of perfluorinated alkanes with short side-chains that are attached with ionic groups (usually Sulfonate (SO_3^-) or carboxylate (COO^-) as shown in Fig.3. Since, as discussed earlier, ionic polymer actuation requires the specimen to be permeable to foreign solvent ions, the permeability of the Nafion based IPMC membrane is caused by the presence of sulfonic acid groups (SO_3^-). In the hydrated state, the positively charged ions or cations get connected with SO_3^- groups and become mobile enabling the polymer to conduct cations [54]. The anions, or negatively charged ions, get attached to the IPMC base membrane matrix while the cations, or positive ions, remain in the fluid in a mobile state. IPMCs swell in the hydrated state because of the ionic and hydrophilic nature of Nafion or Flamion membrane. When the specimen is hydrated, the water molecules on the IPMC surface acts as a medium for ionic migration. Therefore the amount of water present on the IPMC surface plays an important

role in the working of IPMC [10]. IPMCs work suitably in the hydrated state whereas they can also be made as encapsulated membranes to work in dry environment.

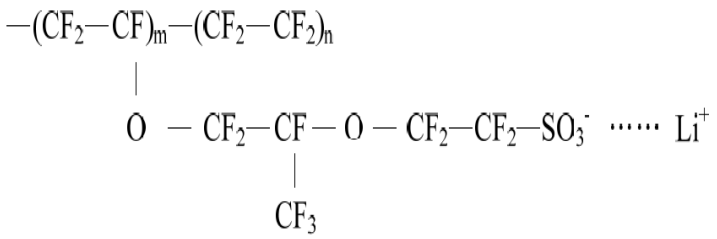

Fig. 3. Chemical structure of a Nafion based IPMC [54]

The permeability characteristics of IPMC's depend heavily on their base ionomeric membranes; Nafion based IPMCs are permeable to cations and water molecules whereas Flemion based IPMCs are permeable only to anions and water. For the case of a Nafion based IPMC, when an electric field is applied across the wet specimen, the diffusion of solvent cations towards the negative electrode results in the bending on the membrane. Typically, the Nafion based IPMC's show a bending movement towards the anode while it's the opposite in the case of Flemion based membranes.

The backbone membrane in IPMCs are designed and manufactured in a specific manner in so that they allow diffusion of mobile cations and water through the nano pores and channels of the polymer matrix; whereas the covalently bonded anions remain fixed in the polymer matrix [54].

1.5. Manufacturing Processes for IPMCs

This section will the discuss techniques used in preparing IPMC specimens. Although there are different ways of manufacturing IPMC specimens, this discussion will be limited to the most popular technique, which was proposed by Oguro [56] for a Nafion based IPMC sample

[56], [10], [4], [14], and [16]. This technique involves four stages between the initial preparations of the material to the final IPMC specimen as outlined next. These stages can be broken down into two distinct processes, the initial compositing and later the surface electroding process; both of these processes lead to different morphologies of precipitated platinum on perfluorinated ion exchange membrane as illustrated in Fig.4. and Fig.5.

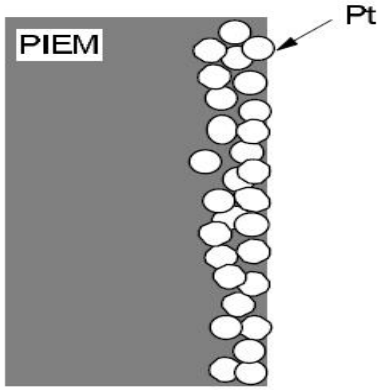

Fig. 4. A schematic diagram showing the initial compositing process

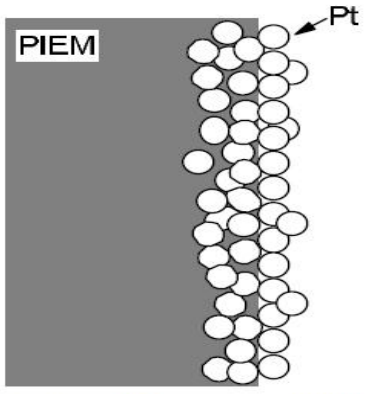

Fig. 5. A schematic diagram showing the surface electroding process

Stage.1. Roughening and Cleaning Process

In this stage the surface of the base material, i.e., Nafion, is roughened to increase the surface area density where the platinum salt penetration will take place before being reduced to platinum as will be discussed next. Roughening is done by sandblasting the dry surface of the base polymer by blowing fine glass beads using compressed air. After mild sandblasting of the membrane, ultrasonic cleaning is done to remove the residues of glass beads from the membrane by washing the membrane using ultrasonically agitated water in an ultrasonic cleaner.

Immediately after ultrasonic cleaning, the membrane is then chemically cleaned by boiling it in diluted hydrochloric acid (HCl) or nitric acid (HNO_3) for around 30 minutes to take out the ions and impurities from the membrane before being rinsed in de-ionized water. Finally, the membrane is boiled again for another 30 minutes more to further de-ionize it and get rid of the acid, which results in swelling the membrane. The roughened and cleaned membrane can be stored in de-ionized water ready for the next stages.

Stage.2. Ion-exchanging Process

This stage is used to initiate the ion exchanging process by immersing the membrane in a metal salt solution in order to inhabit each ion-exchange location with reducible metal. This is achieved by immersing the membrane in a platinum ammine complex solution (salt solution) of either $[Pt(NH_3)_4]Cl_2$ or $[Pt(NH_3)_6]Cl_4$) for typically more than an hour. Although the amount of ion-exchange or adsorption depends upon the type of charge of the platinum ammine complex present in the solution, both these complex solutions provide good environment for forming platinum electrodes. After immersing the membrane in the platinum ammine solution, it is neutralized by adding ammonium hydroxide solution for atleast three hours. The membrane can be left stored in the neutralized solution at room temperature ready for the next stages.

Stage.3. Initial Platinum Compositing Process

This stage is done in order to do the primary plating of platinum on Nafion surface i.e. to put a thin layer of platinum on the membrane by reducing the platinum complex cations to nano-sized metallic form. To do this, the membrane is rinsed with water; and is kept in stirred water with a solution of sodium borohydride ($NaBH_4$) being added to it for seven times spaces at intervals of 30 minutes. Also, during this process the temperature is gradually increased from room temperature to 60°C, which leads to a black layer of nano-size platinum particle being deposited near the surface of the material. The membrane is then rinsed in water and is kept in a diluted solution of HCl for another one hour.

Stage.4. Surface Electroding Process

This process is done in order to put an additional amount of platinum on the initially deposited platinum layer. The membrane is then plated in an aqueous solution of either $[Pt(NH_3)_4]Cl_2$ or $[Pt(NH_3)_6]Cl_4$), which is continuously stirred and maintained at 40°C first while a small amount of ammonium hydroxide is added in the form of either hydroxylamine hydrochloride (NH_2OH-HCl) or hydrazine (NH_2NH_2) solution at intervals of every 30 minutes. While this process is happening, the temperature is gradually increased to 60°C where it is held for four hours, during which grey metallic layers of platinum are formed on the material surface. The process is complete only after the solution is depleted of its platinum content. In order to determine the ending point of this process, the solution is checked by boiling a small amount with a strong reducing agent ($NaBH_4$). If there are any Pt ions left in the plating solution, it will turn the color of the solution into black. If this is the case, process of depositing Pt is continued by adding more (NH_2OH-HCl) (NH_2NH_2). Otherwise, the prepared membrane is boiled in a dilute solution of HCl after washing it with water and is ready for use.

1.6. Potential Applications of IPMCs

As mentioned before, Ionic polymer metal composites show great potential as actuators that can be used in several different environments, particularly in underwater applications. They can also be utilized in different physical forms, for example, as packaged polymers or as ionic liquid diluent based polymers. IPMC actuators offer an attractive choice for applications requiring large actuator displacement with less force, flexibility, low mass and voltages; they are soft when compared to other brittle ceramic EAPs, which is a good characteristic for compliance purposes. IPMC actuators have been successfully shown to work well in a wide range of applications such as medical, industrial, space, and microelectronic machine (MEMS) [5]. Some of the potential applications of IPMC actuators are discussed below:

1.6.1. Robotics Applications

Because of their actuation abilities in wet conditions just like biological muscles do, IPMCs have been the center of attraction towards development of artificial muscles for many robotics applications. Efforts in developing robots that are as close to humans as possible in every way from the physical appearance/abilities and behavior involve, among other things, developments of flexible actuation mechanisms that resemble biological muscles. In that respect, IPMCs show great potential to be used in building such robots. A robotic arm has been designed using IPMC by [66]. This design used a four-finger gripper made up of IPMCs, with hooks provided at the bottom to act as fingernails.

Along the interest in humanlike robots, there also have been interests in other biomimetic robots such as swimming robots [58] where IPMC have been considered. The first commercial application of IPMCs was a swimming fish robot designed and developed by EAMEX [65]. This robot was constructed using IPMC that bends when actuated, and swims without using electric

motors or batteries. It was powered using an inductive coil that was inductively energized from the bottom and the top the of the fish tank. Another conceptual design of a swimming robotic structure was proposed by Shahinpoor [64]. In that structure, IPMC specimens were cut and packaged in a fishlike robotic form; the desired changes in shape and size to preform swimming actions were achieved by consequently applying alternating voltage across the structure. Therefore, a swimming fish robot or a submarine structure with sealed power and signal generating unit can be designed to swim even at deep levels by changing the buoyancy of the structure. Commands using radio signals can be used to control propulsion speed and buoyancy. These noiseless robotic structures can be used for naval applications.

1.6.2. Space Applications

IPMC actuators can work equally well in low temperatures as well as in the vacuum; they remain being highly resilient with good fracture toughness under these extreme conditions. Because of these features, IPMCs are potential candidates for space applications. When the NASA Viking and Mars Pathfinder missions found out that operating environment on Mars caused accumulation of dust particles on the operating hardware's surface, which could affect the long term usage of optical instruments, IPMCs were considered in the design of the required Martin dust wipers. Bar-Cohen with NASA and NASDA (National Space Development Agency of Japan) proposed an IPMC based dust wiper for planetary applications, and was selected as the basic technology for the infrared camera on Nano Rover's window [59].

1.6.3. Medical Applications

The key characteristics of IPMC such as softness, flexibility, and large displacements make them a good choice to be used as replacements for human muscle. Several researchers have worked on this area and have proposed models for artificial muscles imitating human smooth

muscles. The most popular model used several IPMC strips that were attached together surrounding a liquid carrying tube. A simple control unit that selectively actuate each section of this artificial muscle sequentially [60] [61] was used to produce a travelling wave along the muscle, which in turn forced the liquid to flow through the enclosed tube, thereby transporting the liquid in the tube. Artificial intestines, veins, arteries of different range of sizes and shapes depending on the usage [5] can be manufactured using IPMCs in this form [5]. Since Nafion based IPMCs are biocompatible they can directly be used as muscle implants such as metering valves, exo-skeletal human power augmentation and diaphragm pumps [9]. Additionally, since IPMCs work very well in wet environments, they can be employed in robotic devices that are designed to work inside human bodies to perform surgeries or as assistive devices such as artificial ventricular muscles for heart patients with problems related to cardiac muscle functions. IPMC heart compression artificial devices that avoid thrombosis which results when blood flow makes contact with non-biological surface repeatedly have been reported [5].

1.6.4. Micro-Manipulation Application

Micro-electromechanical systems (MEMS) are a rapidly growing field which is applied in areas that are not limited to in micro-manipulation, micro-assembly, and micro-grippers. IPMCs can be formulated as micro- or macro- grippers to act as an actuator in assembling microsystems and in bio-micromanipulation. Assembling Microsystems deal with grasping and manipulating micro-sized rigid and flexible objects, whereas bio-micormanipulation requires working with flexible and fragile micro-objects such as cells, micro-organisms and bacterium. IPMC actuators have advantages of being flexible with the ability of working in wet as well as dry environments, which makes them good candidates in these applications.

IPMCs can also be used in micro-robots; MEMS devices made up of electroactive polymers especially IPMCs are making it possible to manufacture sensor and actuator microarrays, micro-fabrication processes, and disposable micro-bio-sensors [5]. Manipulating and grabbing small objects has always been a challenge, there are no appropriate actuators for the small range of 10-100μm. Electroceramics (piezoelectric and electrostrictive) is a good choice and have been used in many such applications like ultrasonic motors and inchworms. IPMCs are a good alternative because of good displacement they provide which is incomparable to rigid ceramics. MEMS technology comprises of sensors, actuators, electronics and mechanical systems. IPMCs are easily manufacturable and processable which makes them to be utilized in MEMS technology and shows great potential for future research and application [5].

2. PREVIOUS EFFORTS IN MODELING OF IPMC ACTUATORS

2.1. Introduction

Among the important and interesting features of IPMC materials is that of bending when the specimen is subjected to an electrical field; this bending can be utilized in various actuation functions. By special construction, the IPMC specimens can also behave as if they are contracting instead of bending, which makes them act as muscles [30]. Although there is a considerable amount of information about the bending mechanics in IPMC specimens as it was introduced in the previous chapter, the physical principle behind the bending behavior of the IPMC membrane is not completely verified yet. As such, it has not been possible to completely and uniquely express this behavior mathematically. Despite this drawback, there has been a considerable effort invested in developing better electromechanical mathematical models to express the bending behavior of these materials. It is known that the material behavior depends on various internal physical phenomena of the materials itself; for example, internal electrostatic forces; ionic concentration gradients; ionic movements; and water back diffusion processes, all contribute to the physical behaviors of the material. Studies on how interactions of these internal phenomena explain the high strains that develop within IPMC specimens when subjected to electrical fields have shown that there exists some electromechanical coupling within the material. This coupling enables electrical signals to be used in effecting mechanical displacements that eventually leads to the intended mechanical work, such as the displacement of the free section of the specimen. This electromechanical coupling has been studied by many researchers around the globe leading to development of many distinct IPMC models [18] [19] [20] [21] [24].

Currently, these models can be divided into three different groups depending on the criteria used in developing them. The first group, known as black-box models, has models that were developed based on the empirical data of the membrane's input electrical voltages or currents and their corresponding output mechanical displacements or forces. These models are simple, developed by direct one-to-one mapping of the inputs to outputs; their performance is entirely dependent on the sample for which they were intended, i.e., they are a sample dependent models. On the other hand, there is another group of models known as white-box models, which involve very complex modeling procedures. These models are developed by studying the underlying physical and chemical phenomena that occur within the specimen. While these models are more detailed, they tend to be too complex and intractable for use in control applications. In between the black-box group and white-box group models lies the gray-box group of models. These models are derived partly from the physical phenomena of the material as white-box models but are simplified through system identification methods as in black-box models. These gray-box models are easy to deal with in control applications, and have been the subject of most control focused researches on the topic. All models developed so far consider the IPMC membrane as a cantilever beam clamped at one end and loaded with a distributed force. This chapter reviews some of the popular IPMC's electromechanical models that have been proposed in the field.

2.2. Black-Box Models

Black-box models or empirical/phenomenological models were mostly developed when there was not enough knowledge about IPMC dynamics, and there was a strong need for an accurate model in order to explore possible IPMC's applications [25]. The first black-box model was proposed in 1994 by Kanno and coworkers [18], [23], [40]; since then, more researchers

have looked into the problem [19], [38]. In these early models, the actuator's mechanical response to an applied step voltage was modeled using a linear relationship, which resulted in a transfer function of real poles modeling the displacement of the membrane tip (Y_t) as

$$Y_t = Ae^{-\alpha t} + Be^{-\beta t} + Ce^{-\gamma t} + De^{-\delta t} + E, \tag{2.1}$$

where the capital letters A through E and the greek letters α through δ are constants, and *t* is the time. The constants were determined from experimental data of the tip displacement and the applied input step voltage using a least squares algorithm. The values for the constants A through E were individually determined at several different input voltages (0.5V to 1.5V at an increment of 0.1V) and were reported to be in a non-linear relationship with the applied input voltage. This non-linearity implies that IPMCs actuation characteristics cannot be modeled as a linear and time-invariant system [17]. Models based on this formulation had two major limitations. The first limitation was the fact that the model constants were unable to reflect the level of the input voltage, and thus making the model to be dependent on the input excitation voltage [41]. The second limitation was that these models never considered the physical dimensions of the specimen such as length and thickness, which is not practical especially since the length tends to vary depending upon the application.

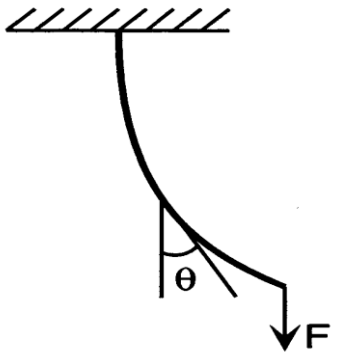

Fig. 6. Actuator configuration for the Xiao and Bhattacharya (2001) model

In another development, researchers Xiao and Bhattacharya proposed another black-box model in 2001 [20]. This new model was centered on the time rate of expansion of the curvature for the vertically suspended IPMC specimen when applied with an input step voltage. A first-order differential equation was used to explain the induced curvature K of the vertically suspended membrane as

$$\frac{dK}{dt} = \frac{1}{\tau}(K_v V - K) \tag{2.2}$$

where the input voltage is represented by V, τ denotes the time constant, and K_v represents the maximum induced curvature per unit of the applied voltage when the applied force is zero. The structure used in developing this model is illustrated in Fig.6; the values of τ and K_v were considered as material properties and were also calculated from the experimental data using curve fitting methods [17].

Another black-box model, which is considered an extension of the Kanno's model of reference [18], was proposed in 2001 by Mallavarapu and Leo in [38]. This model was expressed in a state-space form, which is more control-friendly, as

$$\underline{\dot{x}}(t) = \begin{bmatrix} -\alpha & 0 & \dots & 0 & 0 \\ 0 & -\beta & \dots & 0 & 0 \\ 0 & 0 & \ddots & 0 & 0 \\ 0 & 0 & 0 & 0 & 1 \\ 0 & 0 & 0 & -\omega_n^2 & -2\varsigma\omega_n \end{bmatrix} \underline{x}(t) + \begin{bmatrix} a \\ b \\ \vdots \\ 0 \\ K_r\omega_n^2 \end{bmatrix} u(t) \quad (2.3)$$

$$y(t) = [1 \quad 1 \quad \dots \quad 1 \quad 0]\underline{x}(t) \quad (2.4)$$

where ω_n is the natural frequency, ς is the damping ratio, and K_r is the resonant gain coefficient The values of these constants were found to be dependent on the specimen geometry and the applied voltage. The model was easy to use in designing control systems which resulted in performances that that matched simulation data to experimental data very well in an open-loop system. Linear Quadratic Guassian (LQG) controllers that were designed based on this model had very good performances with diminished overshoot in the step response. Again, despite this performance, the model also was confined to a specific size of the actuator and was not scalable [39].

As would be expected models of this type have an advantage of being easy to understand and implement; however, they are rigidly inflexible and cannot accommodate any changes in the values of the parameters that changes with the dimensions of the transducers, inputs, and outputs as was noted in [25]. Therefore, although Black-Box models are simple to understand and implement, they lack the necessary features required to make them globally applicable to a variety of transducer sizes especially since they don't offer any physical interpretation of their parameters.

2.3. White-Box Models

Models grouped as White-box models are solely designed from the complete knowledge of the physics involved in IPMC actuation processes; they relate the relevant electrical and

mechanical properties of the transducer based upon its physical characteristics [25]. These models are generally based expressed as partial differential equations that explain the phenomenon of the IPMC's mechanical deformation. One of the first white-box models was proposed in 1995 by Shahinpoor [26]; this model, which considered osmotic pressure induced by the electric field as the primary reason for the strain generated in the membrane. The model is generally considered as incomplete because as it was not backed with any experimental results, as such; its validity has not been verified.

The first complete white-box model that was fully solved according to physical laws and compared to experimental results was proposed in 2000 by [27], [28]. Tadokoro and coworkers [27] modeled the Nafion-Platinum composite actuators using six key physical principles: contraction and swelling of the IPMC membrane, motion of ions stimulated by applied voltage, motion of water molecules being dragged by the cations, effects of the momentum and electrostatic force, and changes in the conformation. The model assumed that the balance of force from the mobile cations through the membrane provides a relationship between viscous resistances and the electrostatic force. Viscous resistances are a result of the diffusion forces created by moving cations and water molecules. The flux of concentration satisfying continuity and the net charge are integrated in the force balance. From this balance, a partial differential equation relating the total charge *Q*, the current *i*, and the spatial coordinate *x* was developed as

$$\eta \frac{\partial Q(x,t)}{\partial t} = kT \frac{\partial^2 Q(x,t)}{\partial x^2} + \left\{ kT \frac{\partial \ln \omega(x,t)}{\partial x} - \frac{e}{\epsilon S_x} \left(\int_0^t i(\tau) d\tau + Q(x,t) - Q(x,0) \right) \right\} \frac{\partial Q(x,t)}{\partial x} \qquad (2.5)$$

where, η is the viscous resistance constant, *k* is the Boltzmann's constant, *T* is the temperature, ω is the concentration of water, e is the electric charge on a single cation, ϵ is the dielectric

constant of the hydrated IPMC membrane, S_x is the surface area of the membrane perpendicular to the current flow [39].

The water travel across the membrane was modeled using the equilibrium equation that relates its diffusion forces and its viscous resistance. Under this assumption, the partial differential equation for the number of water molecules *W* was expressed as

$$\eta' \frac{\partial W(x,t)}{\partial t} = kT \frac{\partial^2 W(x,t)}{\partial x^2} \tag{2.6}$$

It was further observed that the migration of cations is principally caused by electrostatic forces, which are stronger than the diffusion forces. The strain in the membrane was assumed to be linearly proportional to the water content, and on the basis of experimental results it was modeled as

$$\epsilon = \alpha C \tag{2.7}$$

where ε is the strain in the membrane, α is a proportionality constant and *C* is the amount of water present. Overall, the interaction between these forces is believed to be responsible for the generation of internal stresses near the anode region in the membrane, which was modeled as

$$\sigma(y,t) = \frac{F_b(y,t)}{S_y} \tag{2.8}$$

where, σ is the internal stress generated, F_b is the electrostatic force on anions, S_y is the surface area that is being considered.

Lastly, the principle of conservation of momentum was applied between the membrane and the hydrated cations, resulting in

$$F_a(t) = M \frac{dU(t)}{dt} \tag{2.9}$$

where, F_a is the reaction force exerted by the IPMC membrane, M is the total mass of the wet membrane, and U is the bending velocity of the membrane [39].

The concluding mathematical model was a system of coupled partial-differential equations relating the applied step voltage to the maximum displacement produced, and few material based parameters which were not directly measurable. Some simplifying assumptions were made, which led to a good agreement between the experimental results and the calculated results [17]. The complexity involved in this model and the assumptions used makes it far less attractive for control applications.

The white-box model proposed by Nemat-Nasser [21] is a revision of what they already proposed in their earlier work [28], but latter focused on the micro-mechanics involved in the actuation. This model considered a general case of the actuator so that different types of cations or backbone structures can be incorporated into the model. The model related the stiffness of the IPMC membrane to the level of hydration by expressing the stress in the IPMC membrane as a function of electrostatic and osmotic pressure within the clusters.

It was assumed that on the application of an electric field, cations redistribute themselves, causing changes in volume in the clusters in each boundary layer, which results in bending the membrane. By formulating the eigenstress rate and membrane's tip velocity as a function of water uptake, the bending motion of the membrane was expressed as

$$\frac{\dot{u}}{L} = \frac{Y_{BL}}{3\bar{Y}_{IPMC} - 2Y_B} \frac{hLL_A}{4H^3} D_A (t_A - \bar{t}_C) \frac{L_A}{L_C} \tag{2.10}$$

where, $\dot{u}$ is the tip velocity of the membrane, L is the membrane's length, Y_{BL} represents the modulus of the boundary layer, h is half of the Nafion membrane's thickness, H is the half of the

thickness of IPMC actuators. In this model, the relation between the young modulus of the composite to the water uptake was assumed to be

$$\bar{Y}_{IPMC} = \frac{Y_M Y_B}{BA_B Y_M + (1 - BA_B) Y_B} \tag{2.11}$$

where, $\bar{Y}_{IPMC}$ is the young modulus for the IPMC membrane, Y_M is the modulus for the metal electrodes, Y_B is the modulus for the bare Nafion membrane, B is the function of water uptake, $A_B$is the concentration factor for the average stress generated in the membrane.

Another white-box model was proposed by Asaka [43]; this model was based on electro kinetically-induced pressure gradient which was assumed to be the main force causing the actuator to bend. This model used a step current as its input instead of the step voltage [39]; it was based on the assumption that water flux in the IPMC actuator is a function of the electro-osmotic flow and fluid pressure gradient. The bending of the membrane is directly related to the stresses in the membrane and the plated layers [39]. Under this formulation, the bending behavior of the membrane was expressed as:

$$\zeta = 2k_1 I\tau_0 \left[1 - \exp\left(-\frac{t}{\tau_0}\right)\right] + k_2 It \tag{2.12}$$

where ζ is the induced curvature, $k_1$and $k_2$are model parameters, I is the current and τ_0 is characteristic time [39].

As seen in these samples, white-box models explain the transduction behavior of the membrane very well but the resulting governing equations are tend to be too complex to be used in control engineering design. For that reason, alternative models have been sought.

2.4. Gray-Box Models

Gray-Box models are based on the well-known physical phenomenon but represent these principles using simple lumped parameter formulations. Since they are designed with enough information about the membrane's operating principles, they lead to the required accuracy while also considering the experimental aspects required to capture the behavior of the membrane. Therefore, gray-box models are less complex and more practical to be used in control applications.

Kanno and colleagues [23] were the first to propose a widely accepted gray box model for IPMC actuators. The actuator was represented in three distinct stages connected in series. The first stage was the electrical stage where the actuator was modeled as a series of simple RC circuit segments as shown in Fig.7. where each segment represents a membrane section of 1mm long [17].

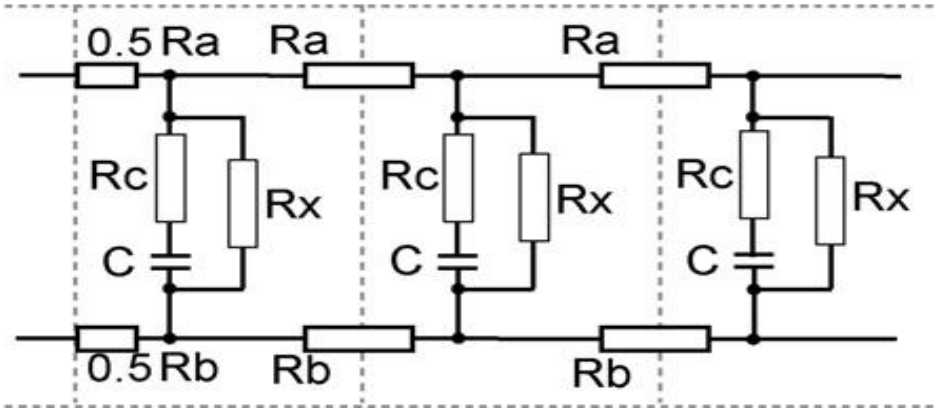

Fig. 7. Gray-box model presented by Kanno et al [17]

The input to the electric stage was the applied electric field, and its output was the electric current; this electric current was used as an input for the next stage. Second stage was the

stress-generation stage where the membrane was further split into three layers through its thickness. The behavior of the stress-generation stage was represented as,

$$\sigma = D\varepsilon - e \left\{\frac{\omega_n^2}{s^2 + 2\zeta\omega_n s + \omega_n^2}\right\}\mathrm{I} \tag{2.13}$$

where, σ is the stress inside the material, D is the mechanical characteristics matrix derived from the polymer's constitutive properties, and $\boldsymbol{\varepsilon}$ is the strain. The induced stress was supposed to be acting on the outer layers only and was calculated by the product of e, the stress-generation tensor, and the current (I). The terms ω_n and ζ represent the dynamics involved in the relationship between the induced stress and current. The final stage was the mechanical stage, where the stress generated from the previous stage acts as the input. At this stage, stress induces contraction and expansion of the surfaces resulting in the bending of the IPMC membrane. This stage was expressed as a dynamic finite element model with proportional damping [17].

Simulation results obtained by using this model compared well with the experimental results. However, this model is still relatively complex, especially if the specimen is more than 5mm long due to the number of RC elements that will be required in the first stage model. Additionally the model assumes the membrane is, considerably long and probably thick so that the effects of its self-weight do not overcome the effects of electrical fields. However for most thin and relatively short specimens, this level of complexity may not be necessary.

Another popular gray-box model was proposed by De Gennes and coworkers in 2000[24]. In developing this model, it was assumed that the water dragged by the migrating ions is the main cause of bending. The application of an electric field E, which causes movement of ions with current density J, was also believed to cause pressure build up Δp due to accumulation of water molecules on one side of the specimen. The reverse process was also believed to be

true, that pressuring the specimen cause water flux Q to flow across the membrane while carrying ions with it. This model could show the basic principles of the direct behavior (actuation) as well as the inverse effect (transduction). The combined transduction and actuation behaviors were represented by the relation

$$J = \sigma E - L_{12}\nabla p \tag{2.14}$$

$$Q = L_{21} E - K\nabla p \tag{2.15}$$

where, σ is the conductance of the membrane, K is the Darcy permeability, and L_{12} and L_{21} are the cross coefficients for the electro-mechanical transduction. The current density, J, is perpendicular to the membrane. These equations model the water and charge transport in the material under steady-state conditions as such, they are unable to account for the membrane dynamics. The phenomenon of water transport this model is based upon has not yet been confirmed to describe the IPMC behavior. This work also models the sensing capabilities of IPMCs as a phenomenon based on the irreversible thermodynamics. The generated electric field E was related to the bending torques Γ on the specimen, by the expression

$$\vec{E} = \frac{12(1-\sigma_p)}{1-2\sigma_p}\frac{L}{\sigma h^3}\Gamma \tag{2.16}$$

where, σ_p is the Poisson's ratio for the material, h is its thickness, and L is its length [63].

Unfortunately, this model was not supported with experimental data. The model also failed to explicitly show the relation between applied voltages to the induced displacement, which makes this model hard to apply in applications of controlling the bending of the membrane using the applied voltage [39].

The grey-box model proposed by Branco [44], explained the bending of IPMC membrane using the continuum electromechanical principles. A lumped-parameter circuit model was derived from the continuum model to calculate the correlation between its current and voltage. This model was designed on a macroscopic level where the effects of water molecules were considered on a very small level compared to the effects of mobile cations in explaining the actuation characteristics of the membrane. The parameters used in the model were identified in its physical meaning and were used to derive and electrical IPMC model as shown in Fig.8.

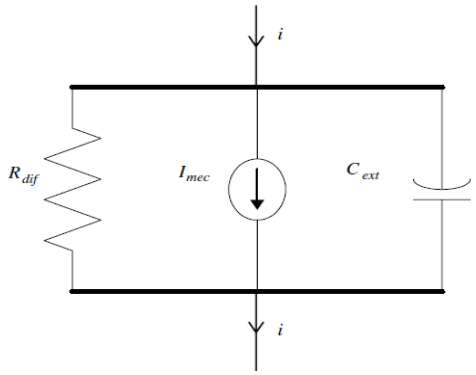

Fig. 8. IPMC electrical model proposed by Branco [44]

At first, the model considers the mechanical characteristics of the IPMC and assumes that mechanical stresses are caused only by electrostatic forces experienced by anions depending on how the cations are distributed. Then the electrical model for IPMC is established in order to determine the electric forces. This helps in determining the cations distribution and thus the electric field intensity. This electromechanical model results in a set of three differential equations,

$$\rho \frac{\partial^2 \delta_2}{\partial t^2} = \frac{1}{2}(x_2^2 - \left(d/2\right)^2) Y \frac{\partial^4 \xi}{\partial x_1^4} + [(2G + \lambda)v - \lambda] \frac{\partial^2 \xi}{\partial x_1^2} + \frac{16Q^2 x_2 (d^2 - 2x_2^2)}{d^4 b^2 l^2 \epsilon} \quad (2.17)$$

$$\frac{\partial \delta_2}{\partial x_2} = v x_2 \frac{\partial^2 \xi}{\partial x_1^2} \tag{2.18}$$

$$i = D_f \frac{8Q}{d^2} + l L_p [\int_0^b (2G + \lambda(v-1)) \frac{\partial^2 \xi}{\partial x_1^2}) dx_1 + Y \frac{d^2}{12} \int_0^b \frac{\partial^4 \xi}{\partial x_1^4} dx_1] + \frac{dQ}{dt} \tag{2.19}$$

where, ρ is the mass density, δ_i is the variable for IPMC's displacement, x_i is the spatial coordinate, d is the membrane's thickness, Y is the Young's modulus, ξ is the transverse displacement in the neutral plane, G is the IPMC's shear modulus, λ is an elastic constant, v is the Poisson's ratio, Q is the electric charge, b is the membrane's length, l is the membrane's width, ϵ is the dielectric permittivity of the Nafion membrane, D_f is the diffusion parameter, and $L_p = \left(\frac{q_+}{Kp}\right)$is available defined for the ratio of electric charge on the ions to a constant.Here, equations (2.17) and (2.18) represent the equation of motion of the IPMC membrane. The equation (2.19) couples the applied electric current and IPMC's displacement.

This model is fairly complex to be used in control applications, and also the electric circuit proposed by this model involves an active current source. However, our assumption suggests that IPMC membrane is made up of passive components only.

3. PROPOSED MODEL

3.1. Motivation for the Model Structure

The proposed model aims to not only capture the IPMC actuator's behavior in a better manner comparable to distributed models, but also keeps it less complex like the lumped parameter models. The IPMC modeling process was started by first collecting extensive data sets on the step voltage applied to the specimen and the observed electric current and mechanical deflection for different specimens varying in sizes.

The IPMC actuator model was developed from a two-step process: first is the development of the electrical model and second is the electromechanical model itself. For the first step of the modeling process, the electric current flowing in the IPMC specimen was monitored for a specific time span. This step was repeated for different settings by varying the applied voltages and the IPMC sample sizes. The time history of the electric current flowing in the specimen at various settings showed that the current in the specimen starts at a high initial value and exponentially reduces to a stable lower value as depicted in Fig.9. This behavior suggested an equivalent electric circuit as shown in Fig.10. with a resistor R_s to determine the high initial current values; R_p to determine the lowest stable current values; and an $R_s C$ branch controls the exponential decay rate of the current.

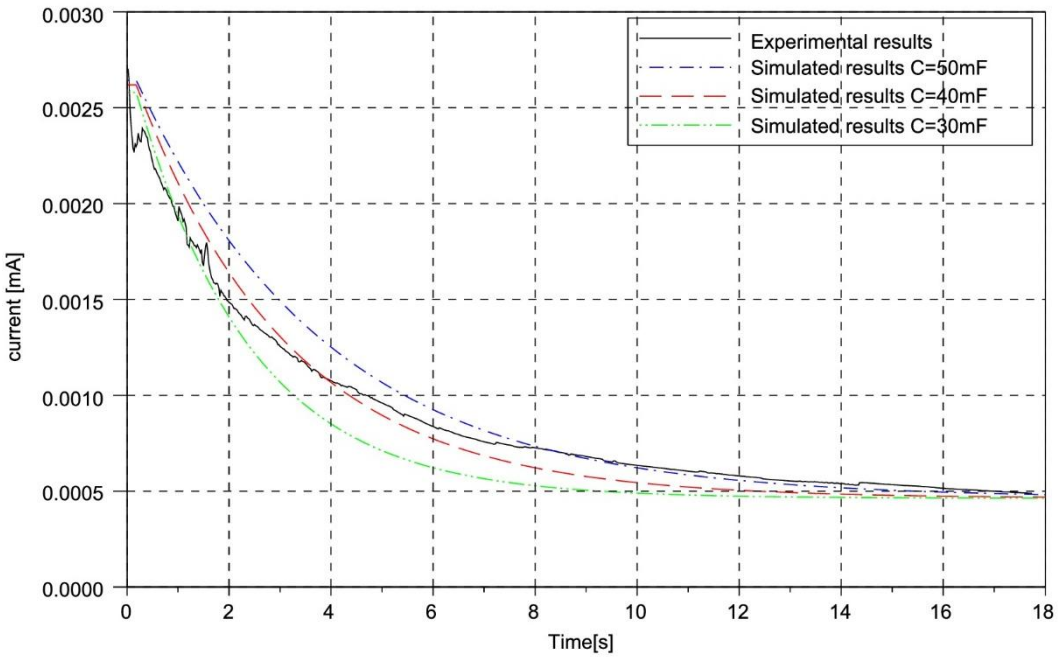

Fig. 9. The current-time history across the IPMC specimen

This behavior of the electric current was observed in all experimental results with different specimens varying in thicknesses and dimensions. The one illustrated in Fig.9. was obtained on a $4\times 1\ cm^2$ Nafion based IPMC membrane with a thickness of 200μm, when applied with a step voltage of 171.4mV. This particular current behavior suggested the values of resistors as R_s=79.4Ω, R_p=351Ω for initial and final current values.

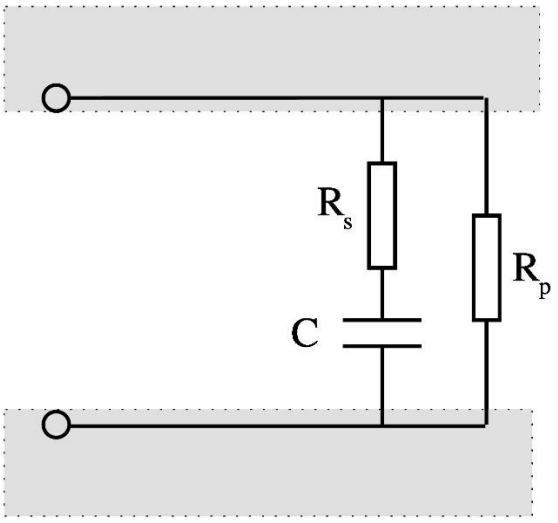

Fig. 10. The proposed lumped parameter RC model of the specimen

As reported in [30], it was noted that the values of *R* and *C* depend on both the degree of wetness of the IPMC specimen as well as the applied voltage. So, the values stated previously are only applicable for an applied voltage of 171.4mV with exact amount of wetness of the membrane and room temperature as when the experiment was conducted.

It was observed that if the values R_s and R_p are kept fixed according to the initial and final current values above, it is highly complex to find out a constant value of the capacitance C to fit the output current profile. This means that during the working action of an IPMC actuator, the value of capacitance and resistance are not constant. This guided us towards the finding that the immigration of ions and solvent molecule in the polymer base matrix frame towards the electrodes decreases the concentration of conducting ions and changes the insulated distance between the electrodes. According to the Fuoss-Onsager theory of electrolytes [31], [32], [33], because of this movement the effective conductance between the two electrodes changes, and therefore, effective resistance and capacitance of the membrane increases.

3.2. The Proposed Electrical Model

The observed behavior of an IPMC specimen can be illustrated as discussed. The IPMC actuator acts as two electrical elements connected in parallel; the first element is the resistance element of the polymer matrix and the plated electrodes altogether, represented by R_p, that can be characterized as

$$R_p = \frac{\rho_m \delta}{A} \tag{3.1}$$

where ρ_m is the resistivity of the polymer matrix, δ is the polymer thickness or the distance between the two electrodes, and A is the area of the IPMC specimen. R_s is the resistance when the specimen is "near dry" and with wetness just adequate to start the start the flow of electric current. The second is the admittance element made up of the solvent and the two plated electrodes with impedance:

$$Z = R_s + X_c \tag{3.2}$$

where R_s is the resistance offered by the solvent and X_c is the resistance of the capacitance C of the polymer matrix, solvent, and the two electrodes. The value of R_s and C depends upon the effective thickness of the solvent, δ_s

$$R_s = \frac{\rho_s \delta_s}{A}, \quad C = \frac{\kappa \epsilon_s A}{\delta - \delta_s} \tag{3.3}$$

here, ρ_s is the resistivity of the solvent, ε_s is the effective permittivity of the area depleted by the solvent under the action of applied voltage. This model is illustrated in Fig.11.

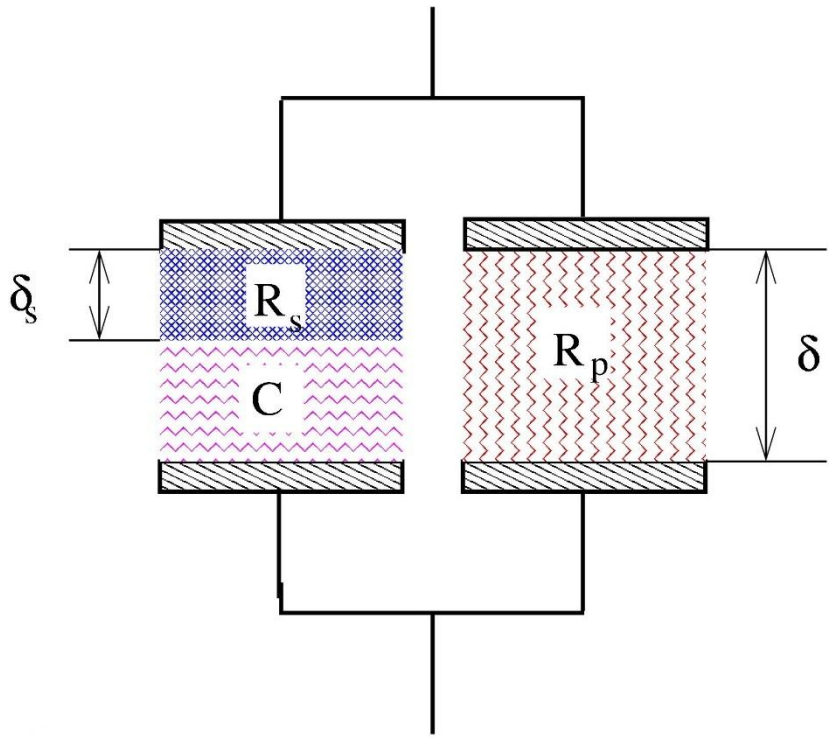

Fig. 11. A simple explanation of the electrical behavior of the specimen

For an IPMC specimen with specific material and size, the resistance value for R_p will remain constant. However, the change in time and flowing current will result in a varying value of the effective thickness of the solvent. Therefore, the values of R_s and C which are dependent upon the value of δ_s, will also change. Also, the changing concentration of the solvent effects the values of effective resistivity ρ_s of R_s and the permittivity ε_s of C; resulting in a time varying values of R_s and C.

The time varying behavior of R_s and C, dependent on δ_s,ρ_s and ε_s, was correlated with the IPMC specimen's ion exchange rates. The popular ion exchange kinetic theories [34], [35] illustrate that during ionic movements, the concentration of ions exponentially changes with time, and reach equilibrium at some particular point of time. In general, the ion exchange rates and growth of [34], [35], can be represented as

$$g(t) = \frac{a - be^{-\beta t}}{c - de^{-\beta t}} \tag{3.4}$$

here, $a, b, c, d \; and \; \beta$ are constants. This is a sigmoidal function, where the growth starts at a predetermined value $\frac{a-b}{c-d}$ and then exponentially increases to $\frac{a}{c}$. The time changing behavior of the parameters δ_s, ρ_s and ε_s also depend on the ion concentration in the medium and should also vary with time as (3.4). The behavior of variations in resistance and capacitance suggested sigmoidal variation too as,

$$\delta_s = \frac{\alpha_{1_\delta} + \alpha_{2_\delta} e^{-\beta_\delta t}}{\alpha_{3_\delta} + \alpha_{4_\delta} e^{-\beta_\delta t}} \tag{3.5}$$

$$\rho_s = \frac{\alpha_{1_\rho} - \alpha_{2_\rho} e^{-\beta_\rho t}}{\alpha_{3_\rho} - \alpha_{4_\rho} e^{-\beta_\rho t}} \tag{3.6}$$

$$\varepsilon_s = \frac{\alpha_{1_\varepsilon} - \alpha_{2_\varepsilon} e^{-\beta_\varepsilon t}}{\alpha_{3_\varepsilon} - \alpha_{4_\varepsilon} e^{-\beta_\varepsilon t}}; \tag{3.7}$$

where, α_i's and β_i's are constants with values so that δ_s is decreasing while ρ_s and ε_s are increasing with time. However, the values of resistivity and permittivity are heavily dependent upon the charge densities, therefore ρ_s and ε_s, which are functions of the ion movements, are expected to be changing relatively faster when compared to ρ_s . By using the models of (3.5)-(3.7) in (3.3), and simplifying it to minimize the number of constants, the values of resistance and capacitances of (3.3) were estimated by sigmoidal logistic functions as

$$R_s(t) = \frac{r_o}{1 + r_1 e^{-\beta_r t}} \tag{3.8}$$

$$C(t) = \frac{c_o}{1 + c_1 e^{-\beta_c t}} \tag{3.9}$$

where ,r_o, r_1, β_r, c_o, c_1, and β_c are positive constants. The values of these constants are a function of the physical properties of the solvent and polymer, and are a ruled by the electrochemistry of both the solvent and the polymer material along with laws of electrodynamics and probability. Also, the values of r_o and c_o also depend upon the present state of the electric current flowing in the IPMC actuator, i.e., the magnitude and direction. As shown in models (3.9) and (3.8), the values of the series resistance, R_s, and the equivalent capacitance, C, will start increasing from an initial value and stabilize at certain value after all the ions and solvent molecules have immigrated accordingly. This change would reverse back to initial values before progressing again to the appropriate stable values under the reversed potential field.

3.3. Experimental Determination of the Electrical Parameters

The values of the parameters used for the electrical modeling were experimentally determined for each IPMC specimen. As discussed earlier, these parameters are affected by a range of factors; this research did not consider those factors. With the aim for the control applications only, it was essential to derive these parameters from the empirical data for an IPMC specimen. Working with the electric current values obtained from step response, the parameters were determined using the least square parameter estimation algorithm.

The current i_s through the $R_s\,C$ branch can be calculated by

$$i_s(t) = V_C(t)\frac{dC(t)}{dt} + C(t)\frac{dV_C(t)}{dt} \tag{3.10}$$

where $V_c(t)$ is the voltage across the capacitor. The electric current i_s saitisfies,

$$R_s(t)V_C(t)\frac{dC(t)}{dt} + R_s(t)C(t)\frac{dV_C(t)}{dt} + V_C(t) = V_s \tag{3.11}$$

where V_s is the voltage across the IPMC actuator. Now, the total current, $i(t)$ can be calculated by

$$i(t) = i_s(t) + \frac{V_S}{R_p} \tag{3.12}$$

At this phase, the model parameters can be calculated by selecting many paths. The approach used in this thesis is based upon the understanding that

$$V_C(t) = V_s - i_s(t)R_s(t), \tag{3.13}$$

which when substituted in equations (3.11) and (3.12) leads to

$$C(t)R_s(t)\frac{di(t)}{dt} + \left(R_s(t)\frac{dC(t)}{dt} + C(t)\frac{dR_s(t)}{dt} + 1\right)i(t) \ldots.$$

$$\ldots + \left(\frac{R_s(t)}{R_p}\frac{dC(t)}{dt} + \frac{C(t)}{R_p}\frac{dR_s(t)}{dt} + \frac{1}{R_p} - \frac{dC(t)}{dt}\right)V_s = 0 \tag{3.14}$$

Now, by again substituting equations (3.8) and (3.9) in (3.14) and simplifying it further, it leads to

$$\Theta\frac{di(t)}{dt} + \Psi(t)i(t) = \phi(t)\mathrm{V_s} \tag{3.15}$$

where,

$$\Theta = c_o r_o \tag{3.16}$$

$$\Psi(t) = 1 + c_1\mathrm{e}^{-\beta_c t} + r_1\mathrm{e}^{-\beta_r t} + c_1 r_1\mathrm{e}^{-\beta_c t-\beta_r t} + \frac{c_0 r_0 r_1 \beta_r e^{-\beta_r t}}{1+\mathrm{r}_1 e^{-\beta_r t}} + \frac{r_0 c_0 c_1 \beta_c e^{-\beta_c t}}{1+\mathrm{c}_1 e^{-\beta_c t}} \tag{3.17}$$

$$\phi(t) = c_0 c_1 \beta_c \mathrm{e}^{-\beta_c t}\left(\frac{1+r_1 e^{-\beta_r t}}{1+\mathrm{c}_1 e^{-\beta_c t}}\right) - \frac{\Psi(t)}{R_p} \tag{3.18}$$

The problem was now solved numerically using dynamic optimization tool in MATLAB [36], to find the values of the parameters that minimize. By using the data experimentally obtained for the electric current $i(t)$ flowing through the IPMC specimen, when applied with a voltage V_s.

For the IPMC specimen discussed in Fig.9., the calculated sigmoid parameters are shown in Table.1., here the capacitance and resistance values are express in Farads and Ohms respectively.

Table 1. Optimal sigmoidal function parameters

c_0	c_1	β_c	r_o	r_1	β_r
0.044	0.1	0.6	91.3	0.1	0.9

Using these parameters, the model capacitance and resistance are predicted to vary as shown in in Fig.12. and Fig.13. respectively. Therefore, the resulting model accurately captured the current flowing in the IPMC specimen as shown in Fig.14.

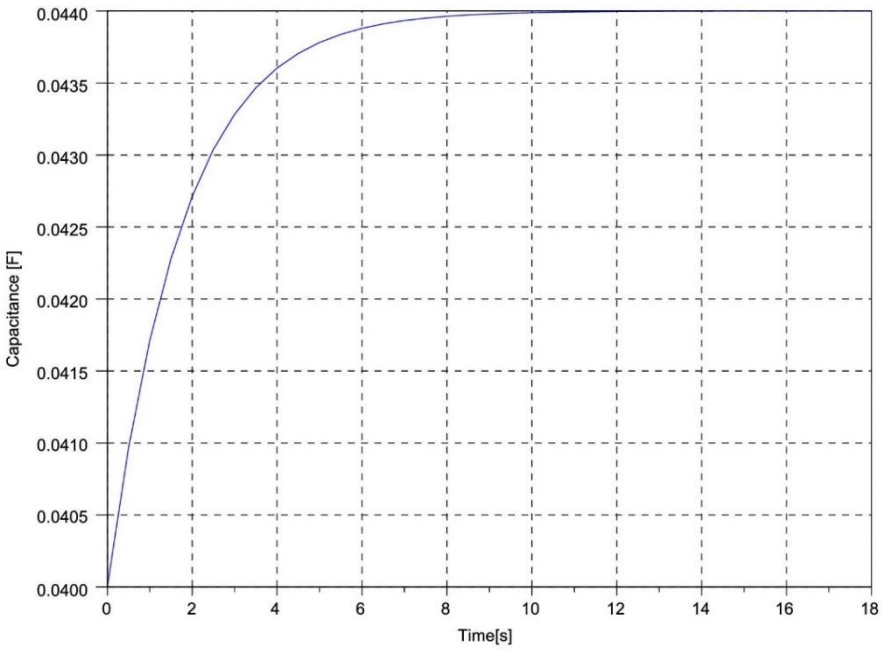

Fig. 12. Variation of capacitance with time

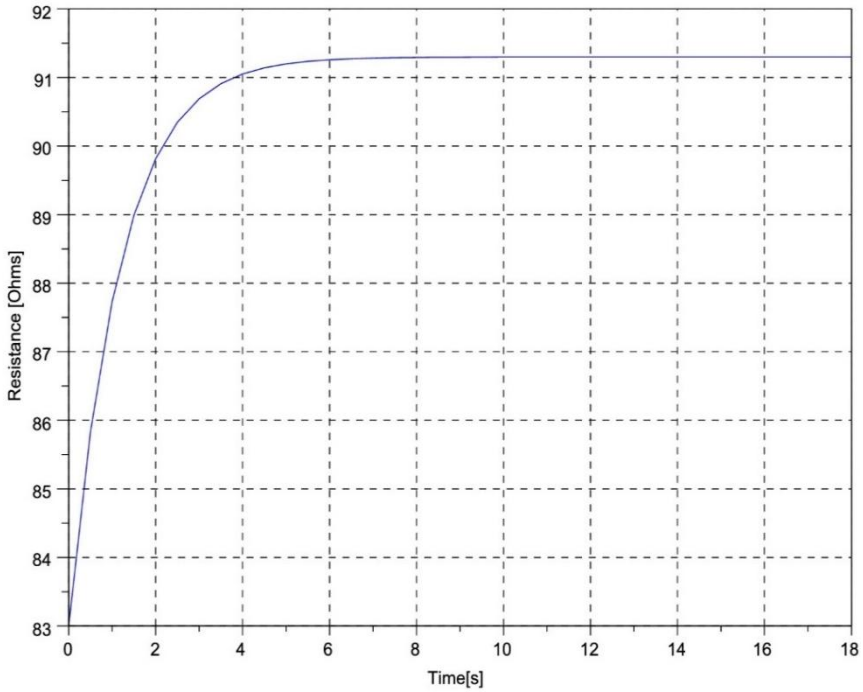

Fig. 13. Variation of resistance with time

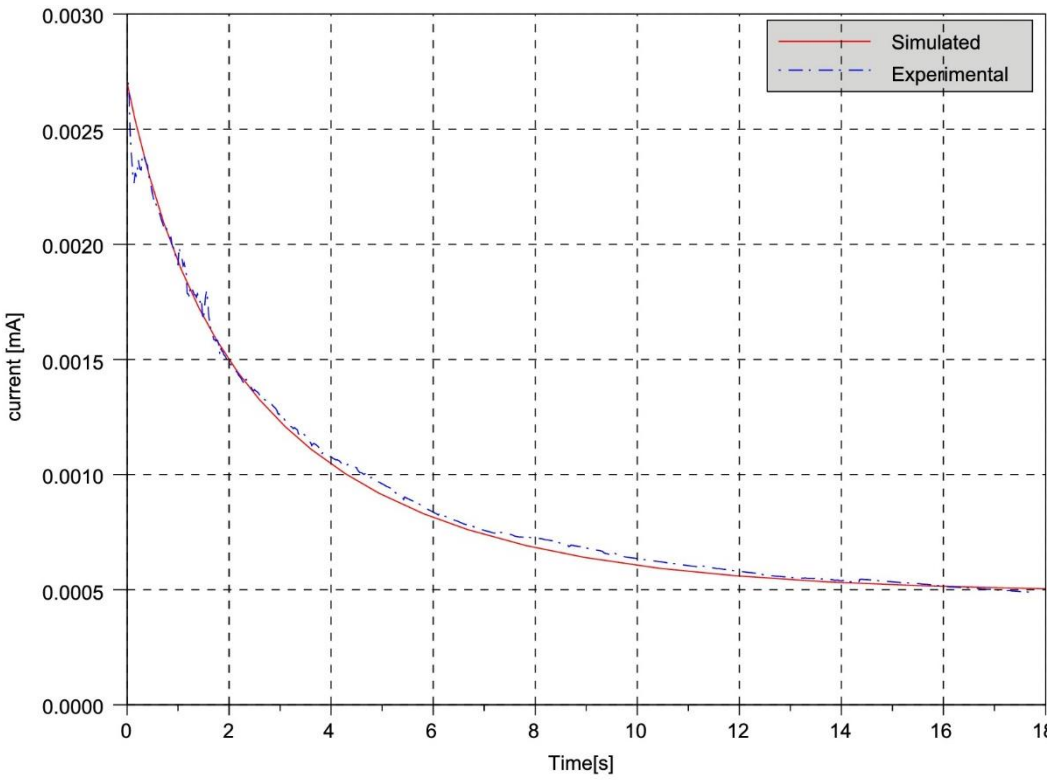

Fig. 14. The current profile through the specimen

3.4. The Mechanical Model and Complete Electromechanical Model

As the solvent ions start migrating and accumulating on one side of the IPMC specimen, the specimen reacts by bending towards the opposite side with lesser solvent concentration. As shown in Fig.15. and Fig.16., the experimental results have illustrated that the bending curvature of IPMC membrane is directly related to the current flowing in the membrane. As seen in Fig.16., the IPMC specimen curvature increases linearly as the current flowing through the specimen decreases, but this observation is not very beneficial for modeling purpose as it relies on the initial and final conditions of the specimen. Therefore, the derivative information was used as shown in Fig.16., which demonstrates that the rate of change of the IPMC specimen deflection is directly proportional to the rate at which current grows through the specimen, i.e.,

$$\frac{dy(t)}{dt} = -\kappa_{y_x}(x,t)\frac{di(t)}{dt} \tag{3.19}$$

where $\kappa_{y_x}(x,t)$ is a constant which depends on the point x along the lenth of the specimen, and the current i.

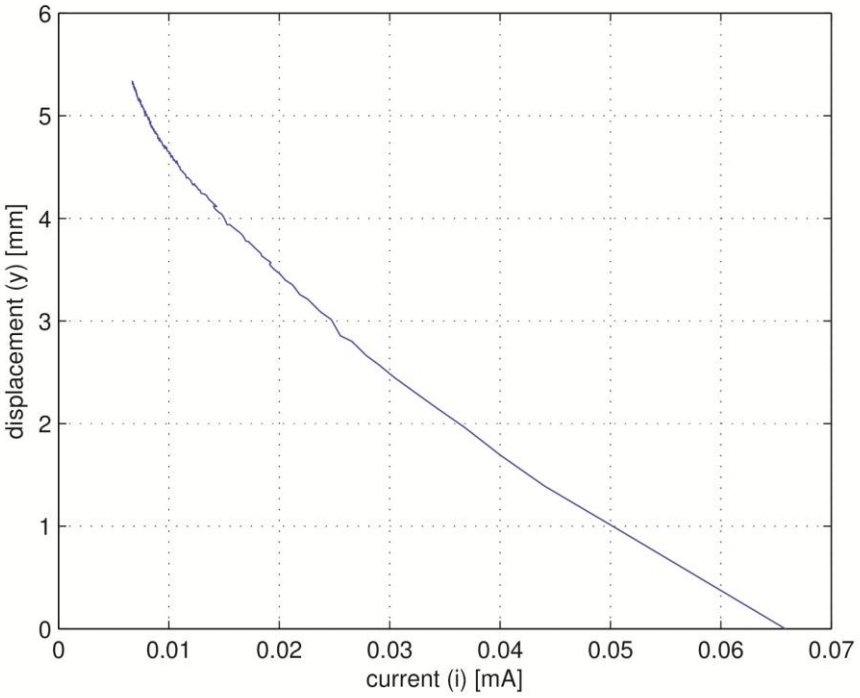

Fig. 15. Variation of the tip displacement against current

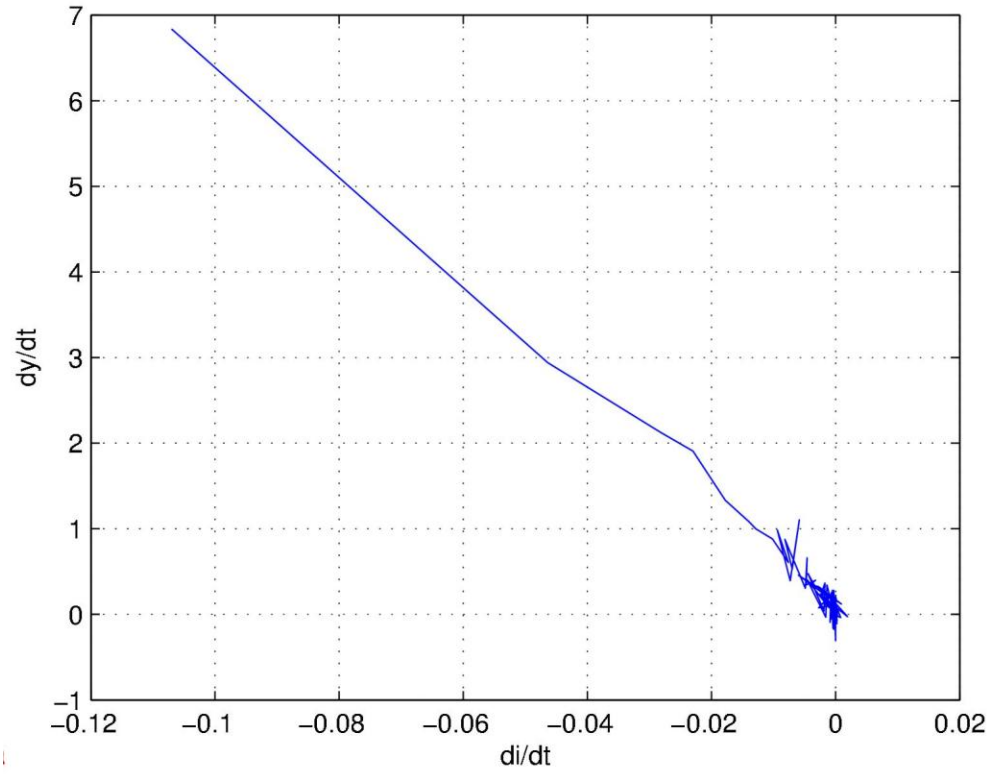

Fig. 16. Variation of rate of curvature against the rate of current

This observation allows the problem to be solved either for the IPMC specimen tip displacement only, or for the displacement of the specimen at any point x along the length. In order to solve for the tip displacement only, the problem can be solved easily by using (3.19) in (3.15) as shown in the next subsection. On the other hand, in order to calculate the deflection at a point x along the length of the specimen, a uniform bending load with an intensity q which is proportional to the current flowing is assumed as shown in Fig.17. This model can be used to control the deflection of any point on the IPMC cantilever specimen and not just the tip deflection.

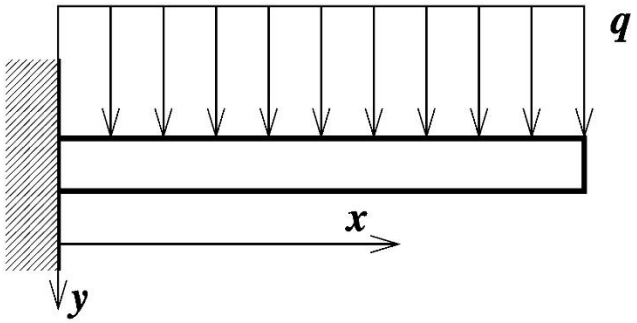

Fig. 17. The cantilever model of the IPMC specimen

Using standard mechanical formulations, the bending moment *M(x)* for this structure satisfies

$$\frac{d^2M(x)}{dx^2} = -q \tag{3.21}$$

since q is proportional to the rate of change of electric current, then the bending moment does not only depend on the position x but also on time t, then this expression can be written as

$$\frac{\partial^2 M(x,t)}{\partial x^2} = -\kappa_M \frac{di(t)}{dt} \tag{3.22}$$

where κ_M is a constant. This bending moment leads to the deflection of the neutral axis with curvature $\lambda_N(x,t)$ at any position x and time t satisfies

$$M(x,t) = \kappa_\lambda \lambda_N(x,t) \tag{3.23}$$

where $\kappa_\lambda$is a constant that involves the Young's modulus and the sectional area moment of inertia of the specimen. There are two things to consider in the bending mechanics of this specimen. First, the resulting deflections exceeds the limits of the assumption that the slope of the neutral axis is negligible; second, the Euler-Bernoulli's beam theory assumption that the plane sections of the specimen remain perpendicular to the neutral axis man no longer be valid

especially since the specimen is made of three layers, which can significantly induce relative shear strains. To address the second observation, the use of Timoshenko's beam theory [69] on the tip deflection $\bar{y}$ leads to

$$\frac{dy}{dx} = \frac{d\bar{y}}{dx} - \gamma_s \tag{3.24}$$

where γ_s is the shear strain in the specimen. However, the thickness of the specimen is normally so small that the effect of the strain may still be neglected without affecting the deflection outcomes.

The curvature of the neutral axis is defined as

$$\lambda_N(x,t) = \frac{\frac{\partial^2 \bar{y}(x,t)}{dx^2}}{\left(1+\frac{\partial \bar{y}(x,t)}{\partial x}\right)^{\frac{3}{2}}} \tag{3.25}$$

where $\bar{y}(x,t)$ is the trajectory of the neutral plane at any position x and time t. If this is combined in (3.23) through (3.24), and neglecting the shear strain, the deflection equation becomes

$$M(x,t) = \kappa_\lambda \frac{\frac{\partial^2 y(x,t)}{\partial x^2}}{\left(1+\frac{\partial y(x,t)}{\partial x}\right)^{\frac{3}{2}}} \tag{3.26}$$

by substituting z(x,t) as

$$z(x,t) = \left(1 + \frac{\partial y(x,t)}{\partial x}\right)^{\frac{3}{2}} \tag{3.27}$$

equation (3.22) can now be written as

$$\kappa_M \frac{di}{dt} = -\kappa_\lambda z^{\frac{-10}{3}}(x,t)\left[\frac{2}{3}z^2(x,t)\frac{\partial^3 z(x,t)}{\partial x^3} - \frac{24}{9}z(x,t)\frac{\partial z(x,t)}{\partial x}\frac{\partial^2 z(x,t)}{\partial x^2} + \frac{56}{27}\left(\frac{\partial z(x,t)}{\partial x}\right)^3\right] \tag{3.28}$$

Using equation (3.28) in equation (3.15) results in a complete electromechanical model that relates the applied voltage to the specimen deflection at any position x and any time. The

curvature can now be directly controlled by using the applied voltage V_s; however, this is a stiff nonlinear dynamical problem that is difficult to control without making some simplifying assumptions as detailed in the next section. Two important observations are made from equation (3.28); the first is that at steady state,t_{ss}, when the current has stabilized, then either $z(x,t_{ss}) = 0$ or when

$$\frac{2}{3}z^2(x,t_{ss})\frac{\partial^3 z(x,t_{ss})}{\partial x^3} - \frac{24}{9}z(x,t_{ss})\frac{\partial z(x,t_{ss})}{\partial x}\frac{\partial^2 z(x,t_{ss})}{\partial x^2} + \frac{56}{27}\left(\frac{\partial z(x,t_{ss})}{\partial x}\right)^3 = 0 \tag{3.29}$$

Since the constraint (3.27) would not agree with $z(x,t_{ss}) = 0$ then only condition (3.29) is consistent with steady state deflection. The second observation is that current starts at the initial current $i_0$and decreases until condition (3.29) is reached, at which point the bending stops and the current stabilizes according to

$$i(t) = i_0 - \frac{\kappa_z}{\kappa_M}\int_0^{t\le t_{ss}} z^{\frac{-10}{3}}(x,t)\left[\frac{2}{3}z^2(x,t)\frac{\partial^3 z(x,t)}{\partial x^3} - \cdots\frac{24}{9}z(x,t)\frac{\partial z(x,t)}{\partial x}\frac{\partial^2 z(x,t)}{\partial x^2} + \frac{56}{27}\left(\frac{\partial z(x,t)}{\partial x}\right)^3\right]dt \tag{3.30}$$

After that observation, we can now focus on the tip deflection again; this approach can be applied at any other point along the specimen. First replace $z(x)$ in (3.29) with its initial deflection of (3.27) again so that

$$\kappa_m\frac{di}{dt} = \frac{15\left(\frac{\partial^2 y(x,t)}{\partial x^2}\right)^3}{4\left(\frac{\partial y(x,t)}{\partial x}+1\right)^{\frac{7}{2}}} + \frac{\frac{\partial^4 y(x,t)}{\partial x^4}}{\left(\frac{\partial y(x,t)}{\partial x}+1\right)^{\frac{3}{2}}} - \frac{3\frac{\partial^2 y(x,t)\partial^3 y(x,t)}{\partial x^2 \quad \partial x^3}}{2\left(\frac{\partial y(x,t)}{\partial x}+1\right)^{\frac{5}{2}}} - \frac{\left(\frac{\partial^2 y(x,t)}{\partial x^2}\right)^3\frac{\partial^3 y(x,t)}{\partial x^3}}{\left(\frac{\partial y(x,t)}{\partial x}+1\right)^{\frac{5}{2}}} \tag{3.31}$$

This equation relates the changing current in the bending membrane to its changing position x along the length of the IPMC membrane.

4. DEFLECTION CONTROL

The IPMC membrane can be precisely controlled using the eletromechanical model proposed in this work. In order to control the tip deflection of the IPMC specimen, the final electromechanical model i.e. equation (3.32) will be combined with the electrical model i.e. equation (3.15) from Chapter III. The formulations will be done using state space, as it is easier to work with for the controlling calculations. Since the deflection $y(x,t)$, slope $\frac{\partial y(x,t)}{\partial x}$, and their higher derivatives in equation (3.32) are independent quantities in time space, i.e., none is a time derivative of the other, then they can be used as independent states for the system. Therefore, we can define the state space as $\mathbb{Q} = \mathbb{R}^5$ where the states $q \in \mathbb{Q}$ are defined as

$$q(t) = \begin{bmatrix} q_1(t) \\ q_2(t) \\ q_3(t) \\ q_4(t) \\ q_5(t) \\ q_6(t) \end{bmatrix} = \begin{bmatrix} i(t) \\ y(x,t) \\ \frac{\partial y(x,t)}{\partial x} \\ \frac{\partial^2 y(x,t)}{\partial x^2} \\ \frac{\partial^3 y(x,t)}{\partial x^3} \\ \frac{\partial^4 y(x,t)}{\partial x^4} \end{bmatrix} \tag{4.1}$$

These states transform the IPMC specimen into a dynamical system of the form

$$\dot{q}(t) = F(q(t), V_s) \tag{4.2}$$

where V_s is the control voltage. To complete the state space model, it was required to create relations among these states. Analysis of data obtained experimentally on states q_2, q_3 and q_4 showed that they all were power functions of time of the form

$$q_i = a_i t^{b_i} + c_i \tag{4.3}$$

where a_i, b_i and c_i are constants that depend on the position x. Since both q_5 and q_6 are x-derivatives of the the former states, then this observation suggests that both q_5 and q_6 also are power function of time. Additionally, by expressing equation (3.32) in terms of q_i and rearranging, so that

$$\mathrm{q_6(t)} = \frac{\kappa_m}{\Theta}(\Phi(t)\, V_s - \Psi(t) q_1)(q_3(t)+1)^{\frac{3}{2}} - \frac{15 q_4(t)^3}{4(q_3(t)+1)^2} + \frac{3 q_4(t) q_5(t)}{2(q_3(t)+1)} + \frac{q_4(t)^3 q_5(t)}{(q_3(t)+1)}$$

…...(4.4)

The number of the power function parameters needed in equation (4.3) can be reduced. For the power function states, a simple mathematical trick that

$$\dot{q}_i = \left(\frac{dq_i}{dt}\right)\left(\frac{q_j}{q_j}\right) = \frac{b_i a_i t^{b_i - 1}}{a_j t b^{b_j} + c_j} q_j \tag{4.5}$$

and the time derivative of equation (4.4) above together lead to a dynamic model of the form,

$$\dot{q}_{(t)} = \begin{bmatrix} -\frac{\Psi(t)}{\Theta} q_1 + \frac{\Phi(t)}{\Theta} V_s \\ \frac{b_2 a_2 t^{b_2 - 1}}{a_3 t^{b_3} + c_3} q_3 \\ \frac{b_3 a_3 t^{b_3 - 1}}{a_4 t^{b_4} + c_4} q_4 \\ \frac{b_4 a_4 t^{b_4 - 1}}{a_5 t^{b_5} + c_5} q_5 \\ \frac{b_5 a_5 t^{b_5 - 1}}{a_2 t^{b_2} + c_2} q_2 \\ \mu(t) \end{bmatrix} \tag{4.6}$$

where the function $\mu(t)$is a time derivative of equation (4.4), i.e.

$$\mu(t) = \frac{\kappa_m}{\Theta}[(q_3(t)+1)^{\frac{3}{2}}\left(V_s\dot{\Phi}(t) + \Phi(t)\dot{V_s} - q_1\dot{\Psi}(t) - \Psi(t)\dot{q_1}(t)\right) \ldots\ldots$$

$$+\frac{3}{2}\sqrt{q_3(t)+1}\,\dot{q_3}(t)((\Phi(t)V_s - \Psi(t)q_1] \ldots\ldots$$

$$-\frac{15}{4}\frac{{q_4}^2(t)\left(3(q_3(t)+1)\dot{q_4}(t) - 2q_4(t)\dot{q_5}(t)\right)}{(q_3(t)+1)^3} \ldots\ldots$$

$$+\frac{3}{2}\frac{q_5(t)\left((q_3(t)+1)\dot{q}_4(t) - q_4(t)\dot{q}_3(t)\right) + q_4(t)(q_3(t)+1)\dot{q}_5(t)}{(q_3+1)^2} \ldots\ldots$$

$$+\frac{{q_4}^2(q_5(3(q_3+1)\dot{q}_4 - q_4\dot{q}_3) + q_4(q_3+1)\dot{q}_5}{(q_3+1)^2}$$

……(4.7)

Therefore, if the constants a_i, b_i and c_i are known, then the problem could be solved directly, however, because of its small size in comparison with the sensor, deflections at only three points were established so that derivatives were numerically reconstructed only up $\frac{\partial^2 y(x,t)}{\partial x^2}$. The power function for tip deflection was found to be

$$y_t = q_2(t) = 7.99 - 5.55t^{-0.2} \tag{4.8}$$

which compares well with the experimental results as shown in Fig.18. Then, by comparing the deflection of two adjacent points, i.e. at the tip and at about 5mm from the tip as shown in Fig.18., the time dependency of the slope of the tip was approximated by a finite differences as

$$\frac{\partial y(x,t)}{\partial x}\Big|_{x=2cm} = \frac{y_{20} - y_{15}}{5} \tag{4.9}$$

where y_{20} is the deflection at the tip, and y_{15} is the deflection at a point 5mm from the tip. This approximation yielded the power function of time as

$$\left.\frac{\partial y(x,t)}{\partial x}\right|_{x=2cm} = q_3 = 0.171 - 0.123t^{-0.2} \tag{4.10}$$

Again, there is a good correlation between the approximated function and the observed experimental data shown in Fig.18. The second derivative of the slope was approximated by using the slopes of the tip at 5mm from the tip, which was computed relative to the origin leading to a power approximation of

$$\left.\frac{\partial^2 y(x,t)}{\partial x^2}\right|_{x=2cm} = q_4 = -0.063 + 0.043t^{-0.2} \tag{4.11}$$

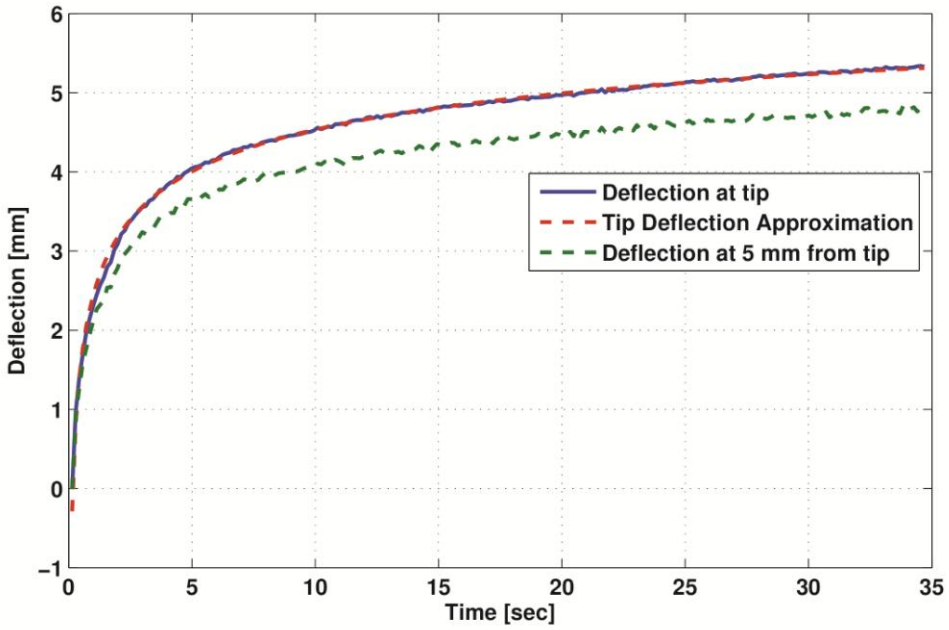

Fig. 18. Comparison of the deflections at the tip and at 5mm from the tip

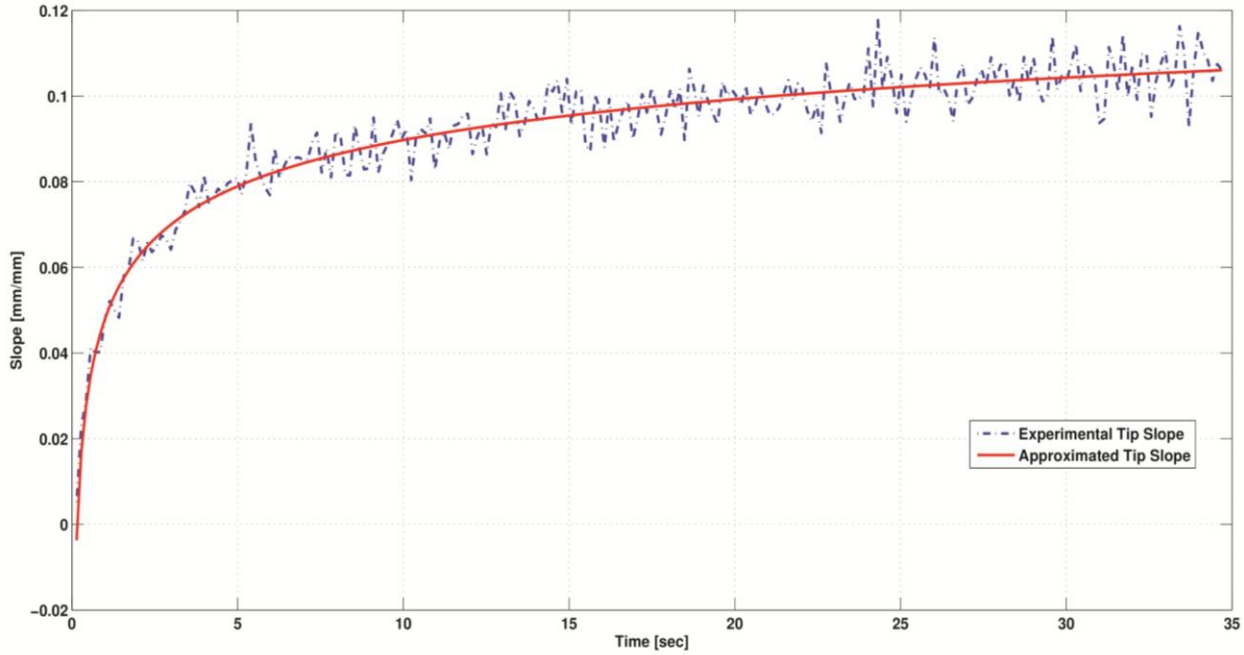

Fig. 19. Approximation of the slope equations

Since the constants the constants a_5, b_5 and c_5 could not be established, some arbitrary value was assumed lumped with some unknown uncertainty Δ such that the true value falls within the bounds of this uncertainty. Since q 5 is linked with other states, it true value could be estimated from the dynamics of the system by a Kalman filter using data from the other states. On noting that the power function parameters decrease with the order of the x derivative, an arbitrary power function for q5 was chosen to be

$$q_5 = -0.008 + 0.01t^{-0.2} + \Delta \tag{4.12}$$

the dynamical system (3.32) with those of (3.15) and (3.32) to result in

$$\dot{q} = F(q, V_s) = \begin{bmatrix} -\frac{\Psi(t)}{\Theta} q_1 + \frac{\Phi(t)}{\Theta} V_s \\ -\frac{1110.0}{\left(124.0t - 169.0t^{\frac{6}{5}}\right)} q_3 \\ \frac{0.0248}{(0.043t^{0.99} - 0.063t^{1.2})} q_4 \\ \frac{0.00903}{(5.55t^{1.01} - 7.99t^{1.21})} q_2 \\ \frac{b_5 a_5 t^{b_5 - 1}}{a_2 t^{b_2} + c_2} q_2 \\ \mu_6(t) \end{bmatrix} \tag{4.13}$$

and $q_5(x)$ is pass through unknown quantity that is estimated by data from other states because of its link in q_5.

The controlled output of course is the tip deflection

$$y = h(q, V_s) = q_2(t) \tag{4.14}$$

To track a particular deflection trajectory, y_r, we set to minimize the trajectory tracking error

$$min \|y_r - y\|_2 \tag{4.15}$$

by using a control law of the form

$$V_s = U(q, y_r, t) \tag{4.16}$$

subject to the dynamic constraint (4.11).

As seen here, this problem can now be handled using standard nonlinear and linear time varying control algorithms. Despite the presence of many states, it is a single-input-single-output system therefore, standard state-space linearization techniques can be used to find the control solution. Note that the system in (4.13) can now be expressed as

$$\dot{q} = F(q) + g(q)V_s + \Delta \tag{4.17}$$

$$y = h(q) \tag{4.18}$$

where Δ represents unknown disturbances and caused by our lack of knowledge on the dynamics of q_5; this formulation fits well in the area of optimal Model Predictive Control [70], [71]. In this simulation results shown in the next section, the control voltage V_s was determined numerically in MATLAB using dynamic optimization tools [36] and Model Predictive control toolbox available from MathWorks.

5. EXPERIMENTAL SETUP AND SIMULATIONS

This chapter will discuss the experimental setup used for the experimental work performed in this work and simulation results to validate the proposed model. Experiments were conducted to get the position response and electric current readings for the IPMC actuator. The IPMC actuator strip position was accurately measured using a laser displacement sensor; the electric current was measured using a simple electric circuit. The measurement was done using DAQ NI-PCI 6014 Data acquisition (DAQ) card which was setup using a LabVIEW program.

5.1. IPMC Specimen Specification

Although Ionic polymer metal composite is a novel material that has been attracting a lot of interest by academia and industry, this material is still in the research and development phase. Therefore it is not yet available commercially and is only fabricated in research laboratories by various research institutions and academia. The IPMC specimens used in this research were cut from several different samples provided by Environmental Robots Incorporated (ERI). There were many similar experiments conducted on different samples varying in the length while the thicknesses were kept the same. Table.2. lists the three sizes of the IPMC strips used in this research.

Table 2. Three sizes of the IPMC strips

Sample	Length	Thickness	Width
A	4 cm	200µm	1cm
B	2 cm	200µm	1cm
C	1 cm	200µm	1cm

All three specimen samples A, B, and C were cut from three different strips provided by Environmental Robots. Fig.20. displays some of the samples of dimension A, B and C used in the experimentation. All the experiments conducted on these samples had IPMCs samples held in a cantilever position.

Fig. 20. IPMC samples A, B, and C

5.2. Laser Displacement Sensor

A laser displacement sensor (OMRON Z4M-W40) manufactured by OMRON Electronic Components, was used to precisely measure the deflection of the IPMC actuator. The laser sensor provides analog output in the range of -4 to 4 V, with a resolution of 10μm and response time of 2ms. It works on the triangulation principle between the receiver and emitter and is capable of measuring bending angle down to around 30º [7]. Fig.21. shows the relation between sensing distance and output voltage of the sensor. The sensor can be powered by using 20V DC.

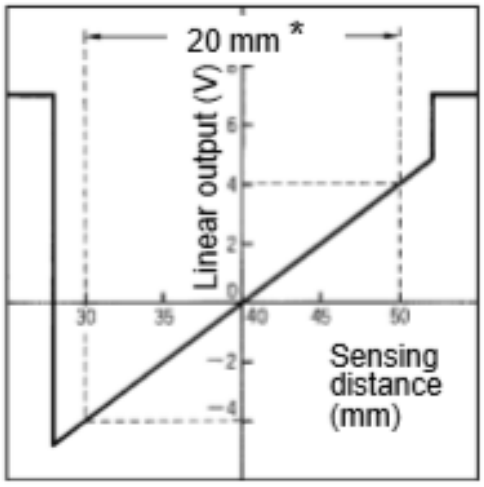

Fig. 21. Sensing distance of OMRON Z4M-W40

When the IPMC specimen is actuated by an applied voltage and it starts bending, laser displacement sensor detects the displacement of the tip of the specimen on the free end of the clamped IPMC strip as shown in Fig.21. The measured position of the IPMC specimen is read by DAQ which converts the analog voltage into digital reading.

5.3. Current Measurement Circuit

A simple circuit was built to accurately measure the current being consumed by the moving IPMC actuator while maintaining minimum resistance. This circuit consists of a 10Ω resistor connected in parallel with the specimen, so that the same electric current flows in both components. The voltage is measured across the resistor and the output voltage is measured using LabVIEW which is reading DAQ's received signals.

5.4. Experimental Setup

Fig.22. shows the schematic of the experimental setup used in all the experiments conducted in this research. The clamp used in these experiments was also provided by the Environmental Robots, these clamps are especially designed with copper electrodes to provide

good contact with the specimen. The IPMC specimen was mounted on an iron platform using the electrode clamp such that the IPMC specimen tip is under the laser displacement sensor's range even after bending as shown in Fig.22.

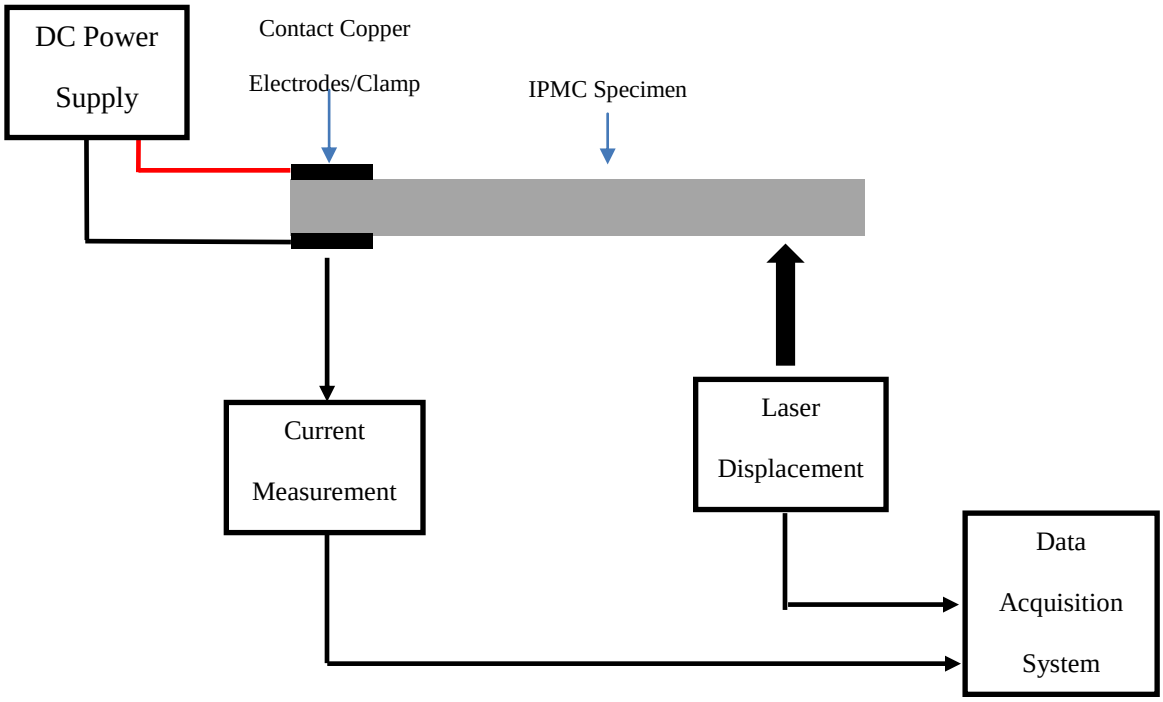

Fig. 22. Schematic diagram of the experimental setup

The output of the laser displacement and current measurement circuit is measured by DAQ system and is further filtered by LabVIEW to remove noise. LabVIEW program also provides filters to remove the unwanted noise in the measured signals. Fig.23. shows the picture of the experimental setup for one of the experiments conducted in this research. The IPMC specimen can be clearly seen clamped between the copper electrode clamps in Fig.24.

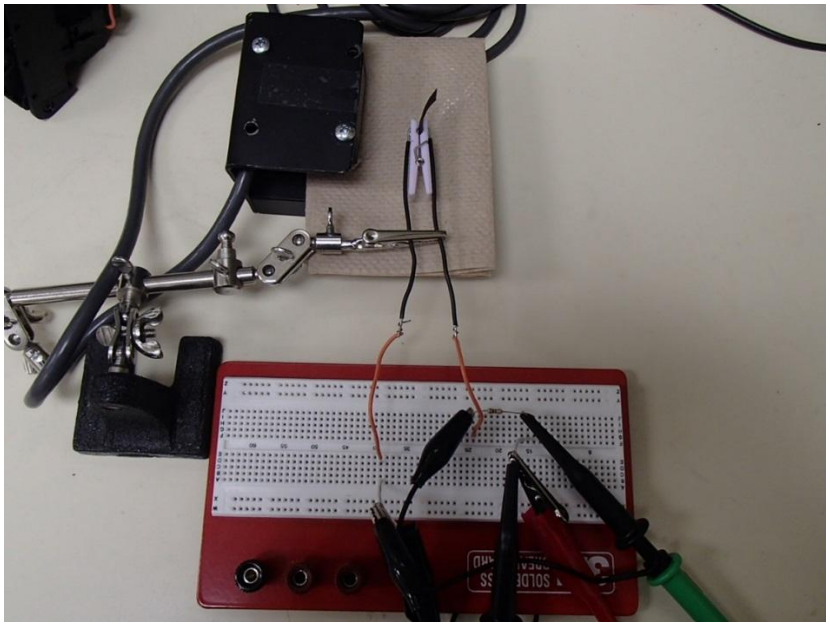

Fig. 23. Experimental setup used for measuring deflection

Fig. 24. Shows an IPMC specimen held by a copper electroded clamp

One of the difficulties that were faced while conducting this research was due to the specimens supplied by the manufacturer expired after being used for several early experimentations. These experiments helped us to formulate our model and get the initial validation experimental results. But as we moved towards the final stage which was validating our work, the IPMC specimens were no longer responsive. This problem was analyzed and while troubleshooting this issue, it was found out that the IPMC specimens were accidentally left in wrong environment for an extended period of time, and hence had lost their actuation abilities. This problem could have been solved by getting some new samples from the supplier but unfortunately the manufacturer was no longer supplying. This led us to validate our model using computer simulations which is discussed in the following section.

5.5. Model Simulations

The proposed model was numerically simulated in MATLAB under both step loading and dynamic loading conditions. The IPMC specimen was a 200μm-thick Nafion obtained from Environmental Robots Inc.; it was cut to 4cm length and 1cm width. The actuation voltage was applied at one end of the specimen while the deflection of the other end was monitored by using the Omron Z4M-W40 laser displacement sensor. The specimen was arranged so that the deflection is confined ion the horizontal plane in order to avoid gravitational effects on the deflection results.

A sample of the results from step loading is shown in Fig.25. where it was required to deflect the tip of the specimen by a normalized displacement of 4.5mm. The control algorithm proposed above suggested a step voltage of 171.4mV to be applied at one end of the specimen. The results in Fig.25. compares the predicted displacements and the actual displacements.

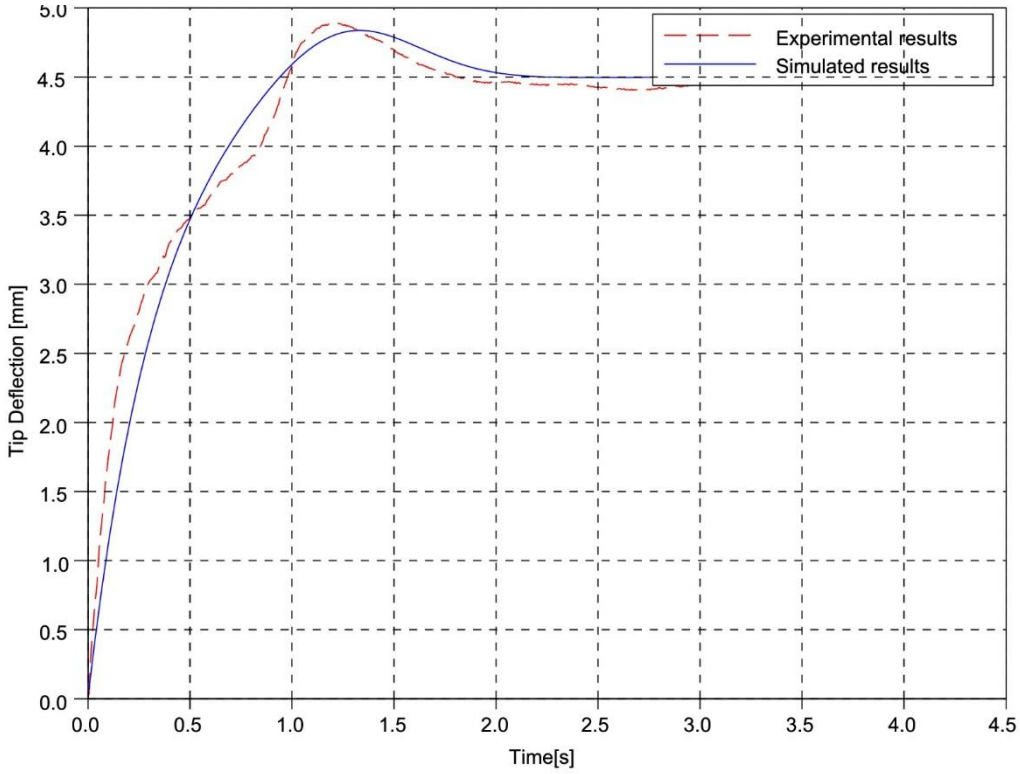

Fig. 25. Deflection of IPMC specimen

These results show that there is a close agreement between the model prediction and the actual behavior of the specimen. In all results collected, it was noted that there is always an overshoot in the deflection of the free end, and the model was able to capture this overshoot especially when the deflection is within the sensor range. Large deflections could not be verified since the displacement sensor has a limited range; all overshoots within the sensor range were captured correctly except those that were out of range. The performance of the model and the control algorithm under dynamic loading is shown in Fig.25 through Fig.26. The tip of the specimen was required to oscillate sinusoidally with an amplitude of 3mm at a frequency of 0.6Hz. The computed control voltage was found to also be a sinusoidal signal of the same frequency as the intended vibration of the specimen, but with amplitude of 150mV. A digital

function generator set with these signal parameters was used in activating the specimen. Fig.26. shows the expected voltage and the signal that was actually applied to the specimen by the function generator. Observed tip deflections for the dynamic loading are shown in Fig.27., where the actual deflections are compared with the computed values.

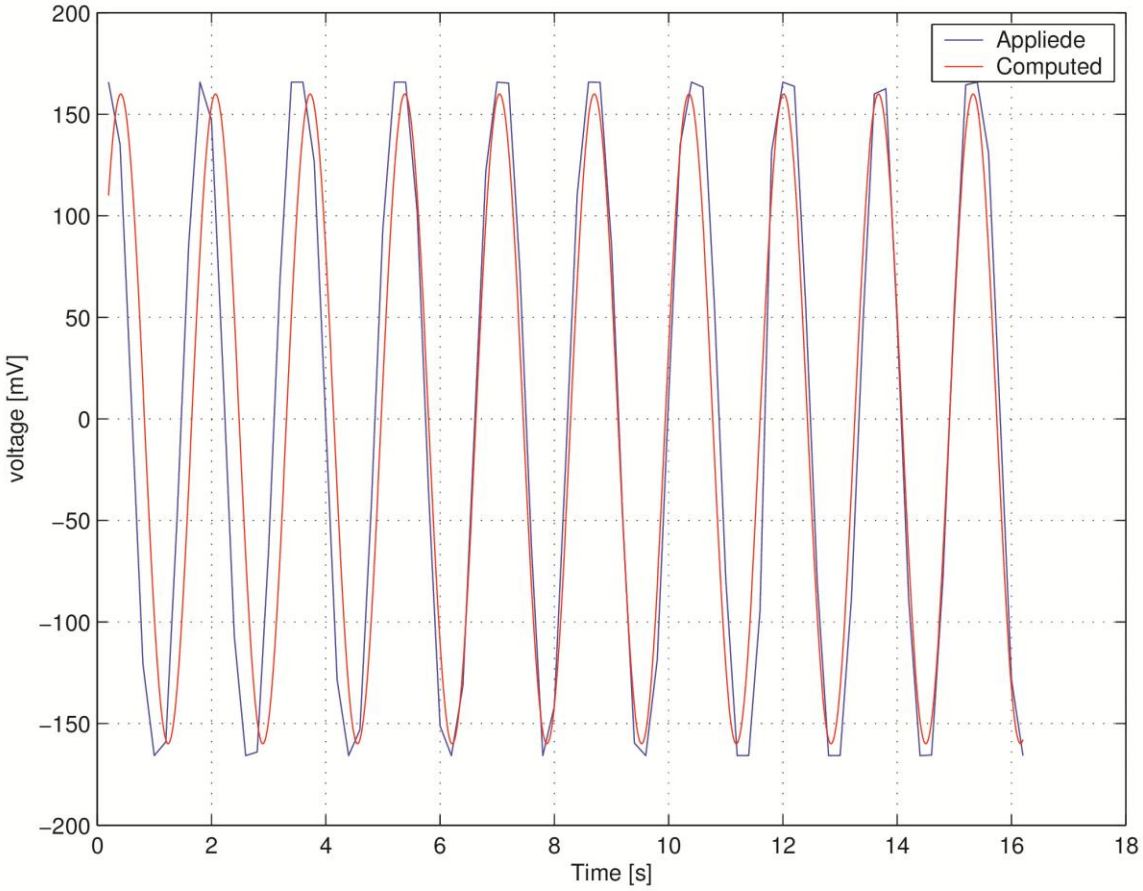

Fig. 26. The computed sinusoidal voltage compared with actual voltage applied to the specimen

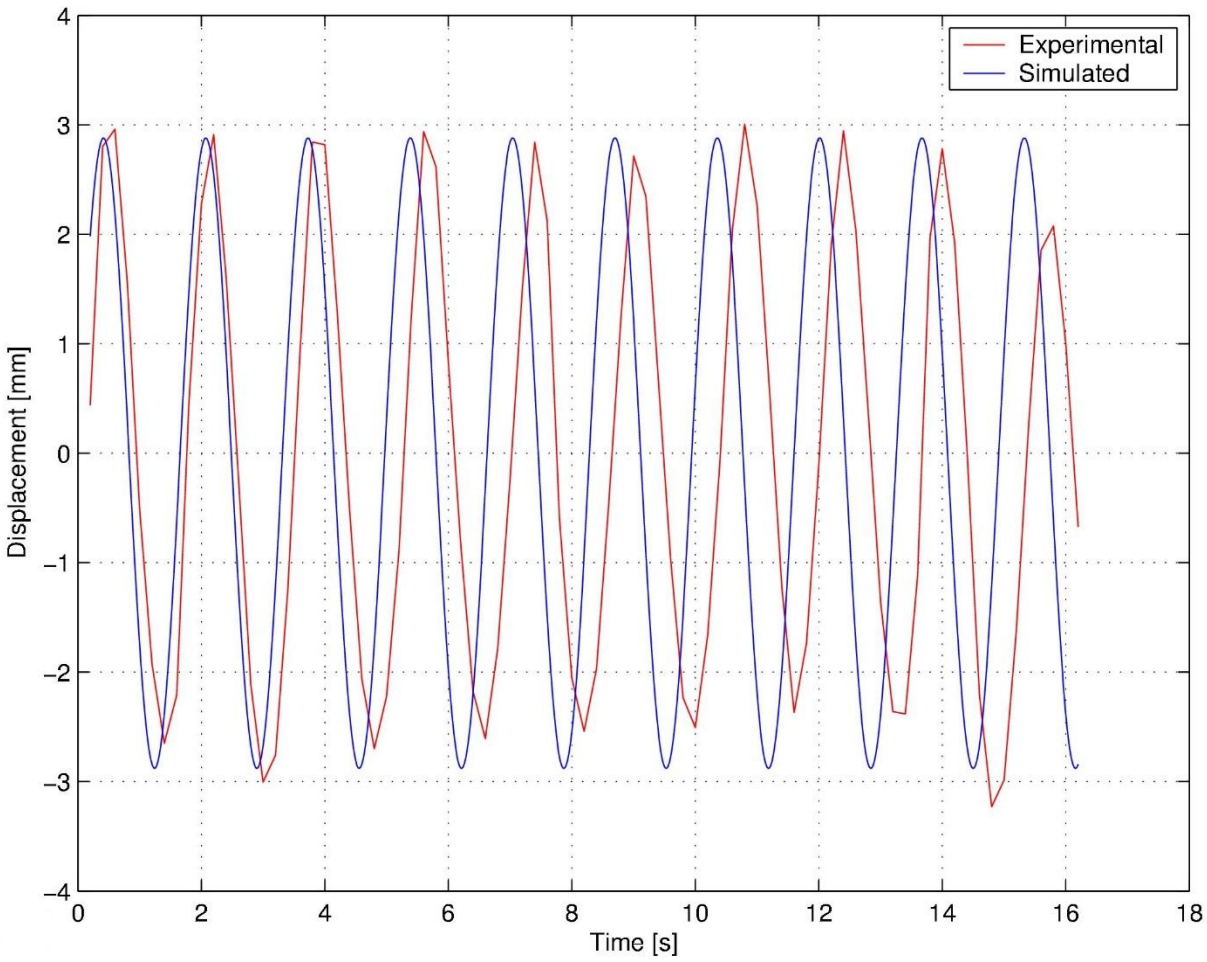

Fig. 27. The comparison of the measured tip deflection versus predicted value

There is an observable delay in the tip response compared to the predicted response. This delay was thoroughly studied and it was found out that the delay was actually caused by the Laser Displacement sensor which is around 2ms (the response time of the sensor as mentioned in section 5.2). This led to some discrepancies between the simulated results and the experimentally received tip deflection data.

6. FUTURE WORK

The electromechanical proposed in this research can be utilized to control the IPMC bending at any position on its length. With the limited availability of the IPMC membrane, this research represented the dynamic control model for the control of the tip displacement. Unavailability of more specimens forced the research abandon some of the work which was crucial to the research. More experimental results of the IPMC bending at different values of the position x will be able to provide exact control dynamics which can be used in controlling the membrane at any position x. Future work is recommended as follows

6.1. Improvement of the Model by Better Power Function Parameters

Further experiments are recommended to determine the displacements at multiple points so that all power function parameters used in equations 4.1 through 4.4 can be determined with certainty. Availability of such parameters will improve the quality of the dynamical model (4.4) which is likely to yield better results.

6.2. Generalization of the Model

The model presented in this thesis is based on short specimens, and all results were left in terms of the absolute displacement. Experimenting with long specimens is recommended and compare various ways of generalizing the results. The results can be generalized by normalizing the displacement per unit length of the specimen such that $\hat{y} = \frac{y}{l}$ Or by normalizing the displacement per unit volume of the specimen $\hat{y} = \frac{y}{Al}$

With sufficient experimental results, it should be possible to compare these two normalization methods and choose one.

7. CONCLUSIONS

This research has proposed a simplified linear electromechanical model which can be used in predicting and controlling the IPMC actuators. The electromechanical modeling part is a combined result of electrical and mechanical models.

The electrical model was developed by evaluating the experimental data obtained from the step voltage response of the IPMC. The passive components used in the electrical model were found out to be varying with time and were predicted using logistic functions. The parameters used in defining the passive electrical components were determined using combinations of laws of electrochemistry of both the solvent and the polymer material, electrodynamics and probability theory. The bending mechanics of the membrane was defined using Timoshenko's beam theory. The bending curvature of the specimen was eventually related to the rate of change of current in the specimen. These two models were combined and was presented as the complete control oriented electromechanical model. Although currently proposed model is still specimen specific, it could be generalized to all types specimens if these deflections are expressed as deflection per unit length or deflection per unit volume.

The electromechanical model was then used to formulate a control oriented dynamic model of a Nafion based IPMC specimen from which an Optimal Control System was suggested for the IPMC actuators.

8. REFERENCES

[1] R.C. Richardson, M.C. Levesley, M.D. Brown, J.A. Hawkes, K. Watterson, and P.G. Walker, "Control of ionic polymer metal composites," *Mechatronics, IEEE/ASME Transactions*, vol. 8, no. 2, pp. 245-253, 2003.

[2] Ujwal Deole, Ron Lumia, Mohsen Shahinpoor, and Michael Bermudez, "Design and test of IPMC artificial muscle microgripper," *Journal of Micro-Nano Mechatronics*, vol.4, no.3, pp. 95-102, 2008.

[3] http://www.innoresearch.net/report_summary.aspx?id=46&pg=119&rcd=ET-106&pd=2/1/2008

[4] M. Shahinpoor, and K. J. Kim, "Ionic polymer-metal composite: I. Fundamentals," *Smart Materials and Structures*, vol. 10, no. 4, pp. 819–833, Aug.2001.

[5] M. Shahinpoor, and K. J. Kim, "Ionic polymer-metal composites: IV. Industrial and medical applications," Smart Materials and Structures, vol. 14, no. 1, pp. 197–214, 2005.

[6] S. Nemat-Nasser, and C. Thomas, "Ionic polymer-metal composite (IPMC)". In *Electroactive Polymer (EAP) Actuators as Artificial Muscles - Reality, Potential and Challenges*, Y. Bar-Cohen, Ed. SPIE Press, ch. 6, pp. 139–191, 2004.

[7] Yun Kwan Soo, *A novel three-finger IPMC gripper for microscale applications,* Doctoral Thesis, Texas A&M University, College Station, TX, 2006.

[8] Griffiths D.J, Development *of Ionic Polymer Metallic Composites as sensors,* Master's Thesis. Virginia Polytechnic Institute and State University, Blacksburg, VA, 2008.

[9] J.S Najem, *Design and development of a bio-inspired robotic jellyfish that features Ionic Polymer Metal Composite actuators*, Master's Thesis. Virginia Polytechnic Institute and State University, Blacksburg, VA, 2012.

[10] N. Bhat, *Modeling and precision control of Ionic polymer metal composite,* Master's. Thesis, Texas A&M University, College stations, TX, August 2003.

[11] M.J Fleming, *Mitigating IPMC back relaxation through feedforward and feedback control of patterned electrodes*, Master's Thesis, University of Nevada, Reno, 2012.

[12] H. Takenaka and E. Torikai and Y. Kawami and N. Wakabayashi, "Solid polymer electrolyte water electrolysis," *International Journal of Hydrogen Energy,* vol. 7**,** no. 5, pp. 397–403, 1982

[13] Millet, P. and Pineri, M. and Durand, R, "New solid polymer electrolyte composites for water electrolysis," *Journal of Applied Electrochemistry,* vol.19, no.2, pp.162-166, 1989.

[14] Kwang J Kim and Mohsen Shahinpoor, "Ionic polymer–metal composites: II. Manufacturing Techniques," *Smart Materials and Structures,* vol. 12, no. 1, pp.65, 2003.

[15] Min Yu and Hui Shen and Zhen-dong Dai, "Manufacture and Performance of Ionic Polymer-Metal Composites," *Journal of Bionic Engineering,* vol.4, no.3, pp.143-149, 2007.

[16] Bhandari, Binayak and Lee, Gil-Yong and Ahn, Sung-Hoon, "A review on IPMC material as actuators and sensors: Fabrications, characteristics and applications," *International Journal of Precision Engineering and Manufacturing*, vol.13, no.1, pp.141-163, 2012

[17] K. Newbury, *Characterization, Modeling, and Control of Ionic Polymer Transducers,* Ph.D. dissertation, Virginia Polytechnic Institute and State University, Blacksburg, Virginia. 2002.

[18] R. Kanno, A. Kurata, M. Hattori, S. Tadokoro, T. Takamori, and K. Oguro,"Characteristics and modeling of ICPF actuator," *Japan-USA Symposium on Flexible Automation,* vol. 2, pp. 691−698, July 1994.

[19] K. Mallavarappu, *Feedback Control of Ionic Polymer Actuators*, Master's Thesis, Virginia Polytechnic Institute and State University, Blacksburg, Virginia, 2001.

[20] Xiao, Yu and Bhattacharya, Kaushik, "Modeling electromechanical properties of ionic polymers," *Proceedings of the SPIE*, Vol. 4329, pp. 292-300, 2001.

[21] S. Nemat-Nasser, "Micromechanics of actuation of ionic polymer-metal composites," Journal of Applied Physics, vol. 92, no. 5, pp. 2899–2915, 2002.

[22] A J McDaid and K C Aw and E Haemmerle and S Q Xie, "A conclusive scalable model for the complete actuation response of IPMC transducers" *Smart Materials and Structures*, vol.19, no.7, pp. 075011, 2010.

[23] R. Kanno, S. Tadokoro, and T. Takamori, "Linear approximate dynamic model of ICPF," *Proceedings of the IEEE International Conference on Robotics and Automation*, vol. 1, pp. 219–225, April 1996.

[24] P. G. de Gennes, K. Okumura, M. Shahinpoor, and K. J. Kim, "Mechano- electric effects in ionic gels," *EPL (Europhysics Letters),* vol. 50, no. 4, pp. 513–518, 2000.

[25] J. W. Franklin, *Electromechanical Modeling of Encapsulated Ionic Polymer Transducers*, Master's Thesis, Virginia Polytechnic Institute and State University, Blacksburg, Virginia, May 2003.

[26] M. Shahinpoor, "Micro-Electro-Mechanics of Ionic Polymeric Gels as Electrically Controllable Artificial Muscles," *Journal of Intelligent Material Systems and Structures*, Vol. 6, No. 3, pp. 307-314, 1995.

[27] S. Tadokoro, S. Yamagami, T. Takamori, and K. Oguro, "Modeling of Nafion-Pt composite actuators (ICPF) by ionic motion," *Proceedings of SPIE, Smart Structures and Materials*, vol. 3987, pp. 92–102, March 2000.

[28] S. Nemat-Nasser and J. Y. Li, "Electromechanical response of ionic polymer-metal composites," *Journal of Applied Physics*, vol. 87, no. 7, pp. 3321–3331, 2000.

[29] C. Bonomo, L. Fortuna, P. Giannone, S. Graziani, and S. Strazzeri, “A nonlinear model for ionic polymer metal composites as actuators,” *Smart Materials and Structures*, vol. 16, no. 1, pp. 1–12, 2007.

[30] M. Shahinpoor, Y. Bar-Cohen, J. O. Simpson, and J. S. J., “Ionic polymer-metal composites (IPMCs) as biomimetic sensors, actuators and artificial muscles - a review,” *Smart Materials and Structures*, vol. 7, no. 6, pp. R15–R30, 1998.

[31] R. M. Fuoss and L. Onsager, “The Conductance of Symmetrical Electrolytes. I. Potential Of Total Force,” *The Journal of Physical Chemistry*, vol. 66, no. 9, pp. 1722–1726, 1962.

[32] T. J. Murphy and E. G. D. Cohen, “Corrections to the Fuoss–Onsager Theory of Electrolytes,” *The Journal of Chemical Physics*, vol. 53, no. 6, pp. 2173–2186, 1970.

[33] R. M. Fuoss, “Review of the theory of electrolytic conductance,” *Journal of Solution Chemistry*, vol. 7, pp. 771–782, 1978.

[34] F. Helfferich and M. S. Plesset, “Ion exchange kinetics. a nonlinear diffusion problem,” *The Journal of Chemical Physics*, vol. 28, no. 3, pp. 418–424, 1958.

[35] E. R. Gilliland and R. F. Baddour, “Rate of ion exchange,” *Industrial & Engineering Chemistry*, vol. 45, no. 2, pp. 330–337, 1953.

[36] A. E. Bryson, Dynamic Optimization. Pearson Education, 1998.

[37] S.Tadokoro and Yamagami, S. and Takamori, T. and Oguro, K, “An actuator model of ICPF for robotic applications on the basis of physicochemical hypotheses,” *Proceedings of the 2000 IEEE International Conference on Robotics & Automation*, April 2000, pp.1340-1346.

[38] K. Mallavarapu, and D.Leo, “Feedback Control of the Bending Response of Ionic Polymer

Actuators," *Journal of Intelligent Material Systems and Structures*, Vol. 12, pp. 143–155, 2001.

[39] Curt S. Kothera, *Characterization, Modeling, and Control of the Nonlinear Actuation Response of Ionic Polymer Transducers,* Ph.D. Thesis, Virginia Polytechnic Institute and State University, Blacksburg, Virginia, September 2005.

[40] R. Kanno, Tadokoro, S., and Takamori, and Oguro, K, "T., 3-Dimensional Dynamic Model of Ionic Conducting Polymer Gel Film (ICPF) Actuator," *Proceedings of the IEEE International Conference on Robotics and Automation*, pp. vol. 3, 2179—2184, 1996a.

[41] 20] P. J. C. Branco and J. A. Dente, "Derivation of a continuum model and its electric equivalent-circuit representation for ionic polymer metal composite (ipmc) electromechanics," *Smart Materials and Structures*,vol. 15, no. 2, pp. 378–392, 2006.

[42] C. Bonomo, L. Fortuna, P. Giannone, S [42] L. Weiland, L. and Leo, D., "Electrostatic analysis of cluster response to electrical and mechanical loadingin ionic polymers with cluster morphology," *Smart Materials and Structures*,

Vol. 13, No. 2, pp. 323–336, 2004.

[43] K. Asaka, and Oguro. K., "Bending of polyelectrolyte membrane platinum composites by electric stimuli, Part II. Response kinetics," *Journal of Electroanalytical Chemistry*, vol. 480, pp. 186–198, 2000.

[44] P. J. Costa Branco and J. A. Dente, "Derivation of a continuum model and its electric equivalent-circuit representation for ionic polymer–metal composite (IPMC) electromechanics," *Smart Materials and Structures,* vol.15, no.2, pp.378, 2006.

[45] Y. Bar-Cohen, "Electroactive Polymers as Artificial Muscles: Capabilities, Potentials and Challenges", Robotics 2000, pp.188-196.

[46] K. Sadeghipour, R. Salomon, and Neogi, S., "Development of a novel electromechanically active membrane and 'smart' material based vibration sensor/damper," *Smart Mater. Struct.,* vol. 1, no. 2, 1992, p. 172-179.

[47] K. Oguro, Y. Kawami, and H. Takenaka, "An actuator element of polyelectrolyte gel membrane-electrode composite," *Osaka Kogyo Gijutsu Shikensho Kiho,* vol.43, no. 1, pp. 21-24, 1992.

[48] Y. Bar-Cohen, Yoseph,"Electroactive polymers: current capabilities and challenges," *Proc. SPIE,* vol.4695, pp.1-7, 2002,

[49] A. Punning, U. Johanson, M. Anton, A. Aabloo, and M. Kruusmaa, "A Distributed Model of Ionomeric Polymer Metal Composite," *Journal of Intelligent Material Systems and Structures,* vol. 20, no. 14, pp. 1711–1724, 2009.

[50] http://ndeaa.jpl.nasa.gov/nasa-nde/lommas/eap/IPMC_PrepProcedure.htm

[51] M. Shahinpoor, "Conceptual design, kinematics and dynamics of swimming robotic Structures using ionic polymeric gel muscles," *International Journal of Smart Materials and Structures,* vol. 1, pp. 91-94, May 1992

[52] Y. Bar-Cohen, S. Leary, A. Yavrouian, K. Oguro, S. Tadokoro, J. Harrison, J. Smith, and J. Su, "Challenges to the application of IPMC as actuators of planetary Mechanisms,"Y. *Proc. SPIE,* Vol. 3987, 2000.

[53] Y. Bar-Cohen, "Electroactive polymer [EAP] actuators as artificial muscles," *SPIE Press*, Bellingham, Washington, 2001.

[54] M. Shahinpoor, "Continuum electromechanics of ionic polymeric gels as artificial muscles for robotic applications," *Smart Materials and Structures*, vol. 3, pp. 367-372, 1994.

[55] Roentgen, W. C., "About the changes in shape and volume of dielectrics caused by electricity", *Ann. Phys. Chem*, vol. 11, pp. 771-786, 1880

[56] M. Mojarrad, and Shahinpoor, M., "Ion exchange membrane-platinum composites as electrically controllable artificial muscles," *Third International Conference on Intelligent Matreials,* SPIE Proc. Vol. 2779, 1996, pp. 1012-1017.

[57] M. Shahinpoor, and Kim, K. J., 2005. "Ionic polymer-metal composites: IV. Industrial and medical applications". *Smart Materialsand Structures, 14*(1), pp. 197–214.

[58] Eamex, "Fish Robot," EAP in action session, SPIE International Conference on Smart Materials and Structures, March 2003.

[59] Y. Bar-Cohen, T. Xue, M. Shahinpoor, J. O. Simpson, and J. Smith, "Flexible, low mass robotic arm actuated by electroactive polymers and operated equivalently to human arm and hand," in Proceedings of ASCE Robotics 98, pp. 15-21, April 1998.

[60] http://ndeaa.jpl.nasa.gov/nasa-nde/lommas/eap/EAP-web.html

[61] http://ndeaa.jpl.nasa.gov/nasa-nde/newsltr/WW-EAP_Newsletter1-1.pdf

[62] E. Carrera, G. Giunta, and M. Petrolo, Beam Structures: Classical and Advanced Theories, ser. EngineeringPro collection. Wiley, 2011.

[63] M. Henson and D. Seborg, Nonlinear Process Control. Prentice Hall PTR, 1997. [Online]. Available: http://books.google.com/books?id=tZceAQAAIAAJ

[64] E. Camacho and C. Alba, Model Predictive Control, ser. Advanced Textbooks in Control and Signal Processing. Springer, 2013. [Online]. Available: http://books.google.com/books?id=tXZDAAAAQBAJ